

Chlorofluorocarbon uptake in a world ocean model

1. Sensitivity to the surface gas forcing

Matthew H. England¹

Commonwealth Scientific and Industrial Research Organization, Division of Oceanography
Hobart, Tasmania, Australia

Veronique Garçon and Jean-François Minster

Groupe de Recherche de Géodésie Spatiale, Centre National de la Recherche Scientifique, Toulouse, France

Abstract. The uptake and redistribution of chlorofluorocarbons (CFCs) CFC-11 and CFC-12 are studied in a series of world ocean model experiments. In part 1 of this study the sensitivity of the simulated CFC distributions to the model parameterization of air–sea CFC fluxes is examined within a control experiment. The control experiment represents a low-resolution ocean model with global coverage and a proper seasonal cycling in surface thermohaline and wind stress conditions. The specification of a surface ocean CFC concentration that is instantaneously in saturated equilibrium with the atmosphere is found to flux too much CFC into the model. Signatures of CFC-11 are found to be grossly overestimated in regions of deep and bottom water formation, both in the surface mixed layer and at depth. The use of a classical air–sea gas exchange formula (even one with a simplified gas transfer velocity that is independent of wind speed) is seen to greatly improve the CFC simulations at depth. In addition, the model reproduces many of the observed trends in surface CFC concentrations; namely, undersaturation in regions of deep convective overturn and near-surface upwelling and supersaturation in the summer mixed layer. In further sensitivity experiments, we consider the effect of sea ice cover in limiting air–sea gas exchange in polar waters. It is found that bottom water in the Arctic Ocean and around the Antarctic continent is significantly reduced in CFC content once regions covered with sea ice are limited to fractional air–sea gas exchange. This more physically meaningful framework is found to further reduce the spurious uptake of CFC-11 and CFC-12 found under a “saturated surface” assumption. In a final sensitivity experiment the gas exchange rate is parameterized using a complete wind speed and Schmidt number dependence. The wind speed dependent gas forcing increases the surface CFC equilibration rate under the subpolar westerlies. On the other hand, the polar and tropical oceans witness reduced CFC uptake under a wind speed dependent flux regime. Simulated ocean CFC concentrations are compared directly with observational data in certain key areas for deep and bottom water formation. It is found that a reasonable representation of oceanic CFC is achieved in the convected water column in the Weddell and Labrador Seas. In contrast, deep waters that have left the convective area with the model ocean currents are found to be deficient in CFC-11 in the North Atlantic Ocean. This is because the model advective timescale for North Atlantic Deep Water (NADW) outflow across the equator is too long compared with observed ocean estimates. The long timescale is not due to unrealistically sluggish deep currents. Rather, the path of NADW outflow includes a loop eastward from the Labrador Sea into the Northeastern Atlantic Basin, effectively increasing the required outflow journey by around 4000 km. This ages the water mass by almost 10 years, thereby yielding significantly lower CFC concentrations in the NADW extension. In addition, the outflow signature spreads too far into the eastern North Atlantic, presumably because the advective process is too broad and the horizontal diffusion too strong at depth. Contrasting the North Atlantic, bottom water CFC ventilation in the Southern Ocean is found to be too strong, even when significant levels of surface undersaturation are simulated in polar waters. CFC-tagged waters flowing into the deep

¹Also at Division of Atmospheric Research, Commonwealth Scientific and Industrial Research Organization, Mordialloc, Victoria, Australia.

South Atlantic basin (from the Weddell Sea formation zone) are too enriched in CFC-11, even when the deep signatures adjacent to the Antarctic shelf remain close to observations. This suggests that the advective timescale for bottom water ventilation is too rapid in the Southern Ocean. In addition, too much convective overturn persists in the Southern Ocean at 55°S–70°S, with unrealistically deep CFC-11 penetration noted at particular longitudes. This is because not enough older (CFC-deprived) water recirculates and upwells into the Southern Ocean. For example, more upwelled circumpolar deep water in the Southern Ocean would weaken the CFC-11 concentrations by contributing to a lower CFC mixture and by suppressing the convective activity in the region. Bottom and deep level CFC signatures are broad and diffuse compared with the real ocean. The broadness of the CFC imprint is due, in part, to the model resolution, which gives any convective event a spatial extent of at least 3.75° longitude by 4.5° latitude and a bottom level CFC signal thickness in excess of 800 m. An important finding of our study is that the vertical convection of unstable waters acts as the efficient tracer ventilator of the ocean system. This has significant implications for numerical studies of the world's climate, since the meridional overturning has traditionally been considered the reason for the ocean's moderating influence during global warming scenarios. Our study suggests that the vertical convection would play a much greater role over the typical timescale for anthropogenic climate change.

1. Introduction

Direct measurements of the concentration of chlorofluorocarbons (CFCs) in the ocean are now routinely used to add information to conventional hydrographic surveys [e.g., Weiss *et al.*, 1985; Wallace and Lazier, 1988; Doney and Bullister, 1992; Gordon *et al.*, 1992; Warner and Weiss, 1992; Fine, 1993; Smethie, 1993]. Like other transient tracers (e.g., tritium, ^{14}C), CFC distributions are useful for gaining insight into the large-scale ocean circulation over decadal timescales. Unlike the majority of ocean tracers (e.g., nitrates, silicates, oxygen, and ^{14}C), CFCs are little influenced by biological processes and are very stable compounds; they therefore serve as unambiguous tracers of the oceanic circulation. In addition, their input functions are significant over the entire ocean, unlike a number of bomb-produced tracers (e.g., tritium) whose atmospheric concentrations favor the northern hemisphere. With relatively well-known atmospheric histories [Bullister, 1989] and solubility properties in seawater [Warner and Weiss, 1985], CFCs can be readily incorporated into general circulation models (GCMs) of the ocean. In this paper we report the preliminary results of some numerical simulations of the uptake and redistribution of CFCs in a world ocean model. Two main topics are pursued in this study, and, accordingly, we divide the report into two parts. The first (part 1) concerns the method of parameterizing the air–sea CFC exchange rate and, in particular, the sensitivity of our modeled CFC distributions to this input function. The second (M. H. England *et al.*, manuscript in preparation, 1994) (hereinafter referred to as part 2) focuses more on the role of the internal ocean circulation and, in particular, how varying ocean model states redistribute the absorbed CFCs in different ways.

Several efforts have been made to include geochemical tracers into ocean circulation models. For example, Sarmiento [1983] included bomb-produced tritium uptake in a model of the Atlantic Ocean north of 20°S. In some preliminary experiments with annually averaged forcing and internal restoring of temperature T and salinity S below 1000 m, he found that the uptake of tritium was, on the whole, too

weak in the ocean model. To correct this problem, he forced the model to artificially convect tritium in regions where deep mixed layers are observed (following the Levitus [1982] mixed layer depth climatology). In its natural state his model remained too inactive in convection to inject sufficient quantities of tritium into the ocean. Maier-Reimer and Hasselmann [1987] and Toggweiler *et al.* [1989a, b] each studied the uptake and redistribution of ^{14}C in GCMs of the world ocean. The Maier-Reimer and Hasselmann [1987] study focused on the simulation of naturally occurring ^{14}C . Toggweiler *et al.* [1989a, b], on the other hand, considered the ability of their model to simulate both the steady state distribution of naturally produced ^{14}C and the time-dependent uptake of ^{14}C produced during the nuclear bomb tests of the 1950s and 1960s. One of the major findings of their study was that a diagnostic simulation (i.e., one where the interior T and S are continuously restored toward climatological data) was somewhat inferior to a purely prognostic run in terms of the amount of ^{14}C taken up by the model. This appeared to be related to the way convection and vertical motions were suppressed in the diagnostic integration. With reduced convection and vertical motion, realistic quantities of ^{14}C could not be injected into the deep ocean. Apart from the above mentioned simulations performed within differing primitive equation models, relatively little work has been carried out on anthropogenic tracer ventilation in ocean GCMs.

There has been one study of CFC-11 and CFC-12 uptake in a world ocean model [Marti, 1992]. However, this study was somewhat limited in terms of both the ocean model and the CFC forcing method used. The study was carried out within an annual mean model with internal restoring terms on T and S . Both these factors tend to limit the model's ability to redistribute the CFCs with depth, since the model neglects the seasonal mixed layer and the restoring terms inhibit vertical exchange. In addition, Marti [1992] only considered one technique for forcing the upper level CFC concentrations. In his study he assumed the ocean surface was saturated with CFC-11 and CFC-12 at any given time. This oversimplification would greatly favor high surface CFC concentrations. In the real ocean, surface CFC con-

centrations have been observed to be more than 40% undersaturated in regions of only partial sea ice cover [Schlosser *et al.*, 1991]. This is possible because the air–sea gas exchange can be greatly limited when sea ice separates the ocean from the atmosphere. Undersaturation of surface CFCs can also occur in regions of upwelling, since older (CFC deprived) waters are brought to the surface [Doney and Bullister, 1992]. If the upwelling rates are strong, then the air–sea gas exchange may not be fast enough to keep the surface ocean levels near saturation. Yet another example is convection, which also results in the entrainment of older (low CFC) water into the surface mixed layer. The CFC ventilation rate over a deeply convected mixed layer would be naturally limited by the air–sea gas exchange process. For example, Wallace and Lazier [1988] found 40% undersaturation of CFCs in the Labrador Sea during the winter of 1986. The low CFC values were found at the surface outcrop of a recently formed 1600-m deep mixed layer. While the convective process homogenized the CFC distribution in the surface mixed layer, it evidently did so at a rate that greatly exceeded the air–sea gas exchange process. The rapidity of convective events (in both the real ocean and in GCMs) sets a timescale that cannot be matched by air–sea fluxes of gases.

When considering ocean model simulations of anthropogenic gas uptake, particularly when the focus is on high-latitude deep water formation and ventilation rates, it is important that the model considers undersaturation processes when formulating the air–sea gas exchange. Otherwise, systematic errors of the order of 50% of saturation level can be introduced into the model solution. Studies of CFC concentrations measured in the ocean normally make some attempt at considering surface saturation levels, particularly when the water mass considered was formed in polar waters [e.g., Doney and Bullister, 1992; Schlosser *et al.*, 1991; Bullister and Weiss, 1983; Wallace and Lazier, 1988]. Constructing estimates of CFC-11 and CFC-12 percentage saturation over the global ocean will require some parameterization; it is one of the goals of this study to examine ways of making such parameterizations and to see how sensitive the model CFC is to the surface forcing technique.

In an attempt to consider these issues within a world ocean model we conduct four different CFC simulations within a given seasonally forced system. The four experiments sequentially employ more realistic surface layer boundary conditions on CFC-11 and CFC-12. In the first experiment we adopt the crude assumption that the ocean equilibrates instantaneously to the time-dependent CFC concentrations in the atmosphere. By the last of the four sensitivity experiments reported our model CFC forcing simulates realistic undersaturations in regions of upwelling and deep convective overturn, enhanced gas uptake over ocean regions with high wind speed, and a parameterization of limited air–sea gas exchange in the presence of sea ice. With these four experiments we monitor the sensitivity of the model CFC distribution to the range of surface level forcing adopted.

The rest of this paper is divided into five sections. We first describe the ocean model and general circulation in sections 2 and 3. Particular focus is placed on the vertical convection, since this represents the most efficient way for atmospheric tracers to enter the deep ocean. In section 4 we describe

parameterizations of the air–sea gas exchange adopted in this study. The model CFC response to the different forcing techniques is then examined in section 5. Finally, section 6 covers the discussion and conclusions.

2. The Ocean Model

The ocean model used in this study is the multilevel numerical model described by Bryan [1969] and adapted to modern vectorizing computers by Cox [1984] and Pacanowski *et al.* [1991] at the Geophysical Fluid Dynamics Laboratory (GFDL). The configuration of our model is virtually identical to that used by England [1992, 1993], only now we include a complete seasonal cycle in surface-forcing conditions. For a more detailed description of the model configuration and the resulting large-scale steady state circulation the reader is referred to these earlier studies. For the present we summarize the essential model features.

The model geometry adopted in our study matches that used extensively within recent coupled ocean–atmosphere numerical studies [e.g., Manabe *et al.*, 1991, 1992; Stouffer *et al.*, 1989]. The model domain consists of a global coverage of the world ocean extending from the Antarctic continent to the north pole. The model bathymetry represents a smoothed version of the real world ocean bottom topography. The model grid spacing is 3.75° longitude by approximately 4.5° latitude with 12 unequally spaced vertical levels. Because the model's horizontal resolution is somewhat broader than the baroclinic radius of deformation at any given latitude, the effects of mesoscale eddies are only taken into account implicitly by approximate closure schemes. The horizontal A_{MH} and vertical A_{MV} viscosity coefficients are taken to be constants independent of depth ($A_{MH} = 2.5 \times 10^9 \text{ cm}^2/\text{s}$; $A_{MV} = 50 \text{ cm}^2/\text{s}$). Vertical diffusion A_{HV} is lowest in the surface layer ($0.3 \text{ cm}^2/\text{s}$), increasing below the thermocline (following Bryan and Lewis [1979]) toward a maximum of $1.3 \text{ cm}^2/\text{s}$ in the deeper model levels. The horizontal diffusivity A_{HH} reflects the ocean's tendency to diffuse more rapidly at the surface than at depth ($A_{HH} = 1 \times 10^7 \text{ cm}^2/\text{s}$ in the surface level decreasing gradually toward $0.5 \times 10^7 \text{ cm}^2/\text{s}$ at depth). Convection is treated implicitly by the model; whenever vertical instabilities are detected, the diffusion rates are increased to simulate complete mixing over the unstable portions of the water column. This vertical mixing homogenizes T-S (and in the CFC runs, CFC-11 and CFC-12) over the model levels originally detected to be dynamically unstable. No parameterization is included for deepening the surface mixed layer by wind-driven turbulence; that is, the convection of vertically unstable waters remains the only way deep mixed layers are formed in the model.

The ocean is forced at the sea surface by seasonally varying climatological boundary conditions of temperature, salinity, and wind stress. The atmosphere to ocean momentum flux is determined from the wind stress climatology of Hellerman and Rosenstein [1983] interpolated spatially onto the model grid and temporally at each time step. The effective surface fluxes of heat and freshwater are implied by restoring the model's surface layer temperature and salinity toward the Levitus [1984, 1986] seasonal climatology (using a Newtonian timescale of $(30 \text{ days})^{-1}$ for T and $(50 \text{ days})^{-1}$ for S). This approach approximates the actual air–sea exchange of heat [Haney, 1971; Hirst and Godfrey, 1993];

although it can overlook certain temperature feedback processes when a change of ocean state is excited [Rahmstorf and Willebrand, 1994]. On the other hand, a restoring boundary condition on salinity is physically inappropriate. A more meaningful boundary condition on salinity would be derived from a surface freshwater flux [Welander, 1986]. However, available climatological data for evaporation (E) and precipitation (P) remain extremely unreliable, even in well-measured regions. The task of constructing a good seasonally varying global E – P climatology may not be completed for several decades.

Apart from including a seasonal cycle in our sea surface conditions, the ocean model studied carries few of the embellishments available for improved T-S representation. This contrasts with our previous study of water mass formation in a global model [England, 1993]. For example, temperature and salinity are mixed horizontally and vertically without regard for the orientation of isopycnal surfaces. No artificial enhancement of the wintertime conditions is made to excite realistic deep and bottom water production. Instead, the seasonally forced model is integrated out to an equilibrated solution as is. Without the deep acceleration techniques used routinely in annually forced models, almost 5000 years of integration are required before T and S meet the equilibration criteria of England [1993]. The equilibration process is rather more rapid for the ocean circulation than for the thermohaline parameters. Nevertheless, because of the critical role of convection in the uptake rate of anthropogenic CFC, it is important that there be no significant trend in the deep and bottom T-S fields. Seasonal oscillations are noted in the surface 1000 m, mostly due to the annual cycle in convection conditions. Below about 1500 m, negligible variations in T and S occur interannually and only small variations are measured from one season to the next.

3. Model Ocean Circulation and Vertical Convection

Two parameters of ocean circulation of particular interest for the timescales resolved by anthropogenic tracers are the vertical velocity and vertical convection. Together, these parameters define the deep ocean uptake rate of atmospheric gases. The model horizontal circulation becomes important when considering the fate of recently ventilated waters; for example, the southward outflow of recently formed Labrador Sea Water (LSW) is defined by the model advection field at about 1600 to 3000 m depth in the North Atlantic. A synthesis of vertical and horizontal motion is found in a map of the model meridional overturning. Exact ventilation rates must, however, be calculated from the exact velocity fields since the timescale for ocean circulation is determined not by net transport rates but by ocean current speeds. Nevertheless, the merging of two circulation aspects in the one map makes the meridional overturning a useful diagnostic of our model ocean circulation. Along with the convection patterns in the model, the CFC redistribution can be explained simply in terms of these two circulation diagnostics. Two caveats should be mentioned concerning vertical tracer communication in the model. First, the model parameterization of convection does not strictly involve a circulation; tracers are mixed vertically outside any calculation of vertical motion. Secondly, the vertical motion itself is not a

prognostic variable of the model; it is simply determined diagnostically through the continuity equation.

Meridional Overturning

The annual mean meridional overturning in the ocean model is mapped in Figure 1, along with a summer minus winter map to indicate seasonal variability in the meridional cells. The ocean model circulation in the control run is largely similar to the experiments of Toggweiler *et al.* [1989a] and England [1993], since our model geometry and resolution are unchanged from these studies. The one important difference is that our control run includes a seasonal cycle in surface thermohaline and wind stress forcing. The seasonal changes in surface wind stress result in a convergence of surface water in the winter hemisphere (as shown by Bryan and Lewis [1979]), driven by a flux of thermocline water from the summer to winter hemisphere (Figure 1c). Because of this, there is a divergence of water in the summer hemisphere, which results in stronger upwelling, and a deep recirculation from the winter to summer hemisphere. On the annual average, however, meridional circulation closely resembles that in the annual mean models (see also part 2). While the production rate of North Atlantic Deep Water (NADW) is realistic at 20.1 Sv, only 8.5 Sv flows out into the Southern Ocean. This is joined by 5.3 Sv of recirculated bottom water originating in the Weddell Sea (Figure 1b). A total of 26.0 Sv of Antarctic Bottom Water (AABW) is overturned off Antarctica, the majority upwelling south of 60°S. Seasonal changes in the thermohaline overturning rates remain curiously small (~1 Sv variation in NADW production and ~0.5 Sv variation in AABW). This contrasts the rapid response of the model overturning to the shifting wind stress field. Evidently, the deep overturning responds to changes in convective intensity more slowly than the seasonal timescale (3 to 6 months), whereas surface Ekman transports and divergences in flow respond rapidly to the wind stress cycling.

Vertical Convection

In the context of CFC uptake simulations the convective activity of the model is somewhat more important than the meridional overturning. This is because the timescale for convective adjustment in the ocean (hours to days) is much more rapid than the timescale for vertical motion. For example, the vertical motion (or meridional overturning) would require just over 30 years to take some surface level information (e.g., newly introduced CFCs) to 1000 m depth, based on a generous scale vertical velocity of 10^{-6} m/s. Convection in the model efficiently homogenizes entire unstable water columns during just one time step (i.e., just over 1 day). The meridional overturning maps are more relevant, in the CFC context, for showing ventilation rates from regions of convective activity (e.g., the outflow rate of NADW).

The seasonal nature of the surface thermohaline conditions manifests itself in an analysis of the depth of surface layer convection (Figure 2). Convection during the northern hemisphere winter occurs virtually exclusively in the North Atlantic and North Pacific Oceans, with much deeper convective events (up to 750 m depth) in the North Atlantic. During this time, Southern Ocean convection is limited to a small shallow region in the south Indian Ocean and a curiously deep overturn in the Ross Sea. Summertime conditions clearly stabilize the majority of the Southern Ocean,

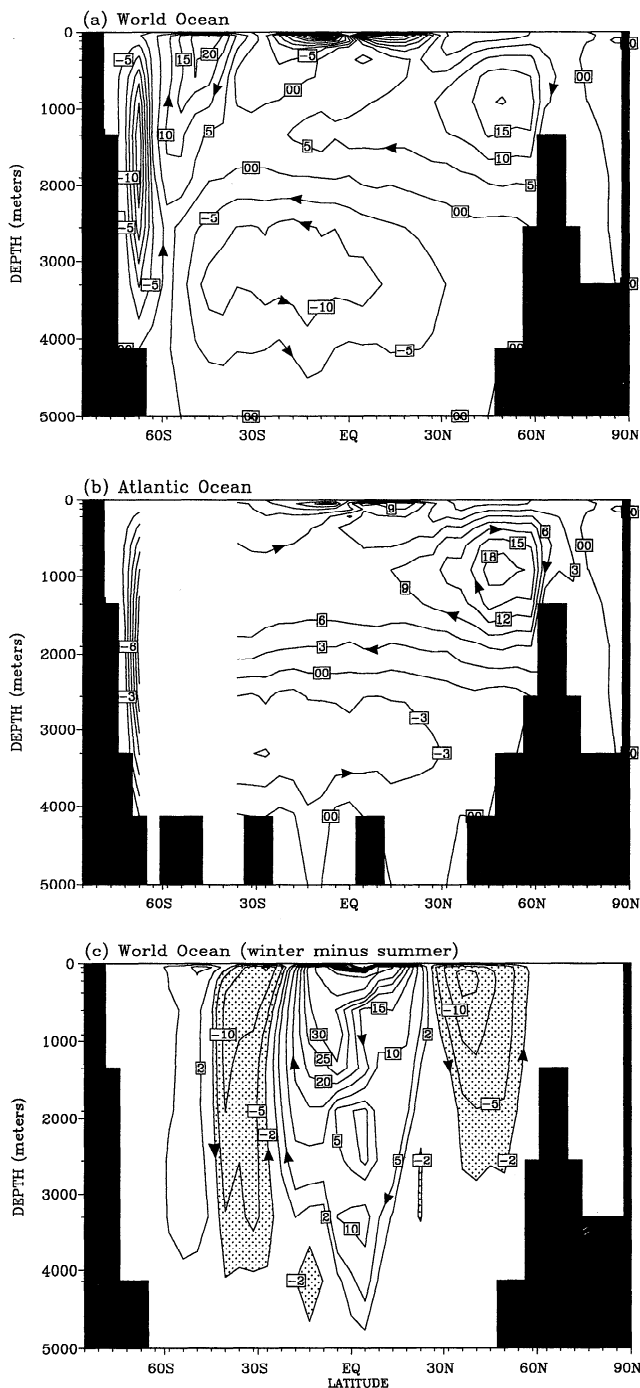


Figure 1. Annually averaged meridional overturning in the control model simulation for the (a) global ocean and (b) Atlantic ocean. No contours are drawn in Figure 1b where the model ocean is free to exchange mass zonally. (c) Difference between the global meridional overturning during the northern hemisphere winter (January–March) and that during the northern hemisphere summer (July–September). Contours are drawn at 5 Sv intervals in the global maps (with extra contours at ± 2 Sv in the difference map) and 3 Sv intervals for the Atlantic sector plot.

with mixed layers rarely deeper than the first model grid level. The Ross Sea exception could indicate poor surface forcing data in the Levitus [1984, 1986] climatologies. This is discussed further in part 2.

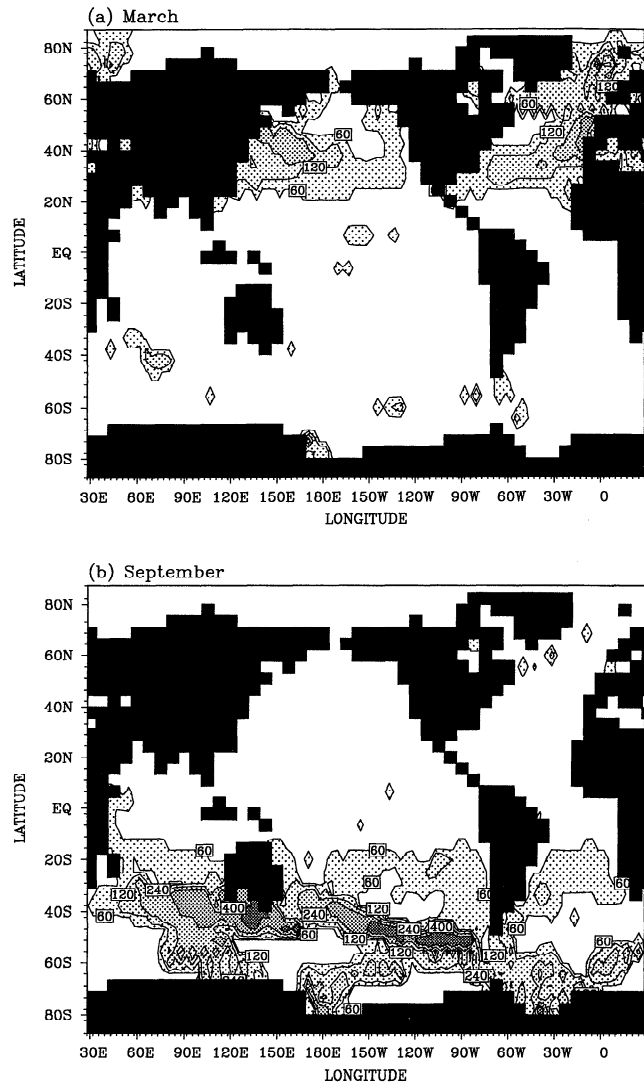


Figure 2. Monthly mean depth of surface level convective overturn (in meters) during (a) March and (b) September. Regions with mean convection depth greater than 60 m (indicating convective adjustment over at least the upper two model levels) are stippled. Stippling density increases with deeper convection depths.

The southern hemisphere winter offsets deep convection in a broad region of the Southern Ocean (Figure 2b). Deep convective layers of more than 1000-m thickness are found in the Ross and Weddell Seas during July to October. A band of convective overturn in the South Pacific Ocean progressively deepens from east of Australia toward Cape Horn, with 750-m thick mixed layers being convected in the southeast Pacific Ocean. The time evolution of this convective band (not shown) reveals that the convection begins near 150°W during June and gradually spreads eastward (at a speed of about 15° longitude/month or 0.45 m/s) to join a convective region near the Drake Passage. This rate of spreading of the convective region matches the speed of surface currents in the region, indicating some role of the surface circulation in offsetting the convective instability [cf. England et al., 1993]. By September the entire band of convective overturn appears. This band of convection is important for the formation of Subantarctic Mode Waters

Table 1. Experimental Design

Experiment	Integration Time	Surface Forcing
Control	4750 years	Seasonally varying T-S and wind stress
CF1	1930–1988	Surface chlorofluorocarbons (CFCs) 100% saturated ($CFC_w = \alpha_c CFC_{atm}$)
CF2	1930–1988	Constant gas transfer speed ($k_2 = 10.6$ cm/h)
CF3	1930–1988	Sea ice cover included [$k_3 = \bar{k}_2(1 - R)$]
CF4	1930–1988	Wind speed dependent k_c [$k_4 = k_o u^2(1 - R)/(Sc)^{1/2}$]

The physical ocean state is integrated over almost 5000 years (without using deep acceleration techniques). The transient CFC simulations are conducted over much shorter periods (around 60 years), corresponding with an integration during 1930–1988. Here CFC_w is the sea surface CFC concentration, α_c is the solubility of CFC in seawater, CFC_{atm} is the atmospheric dry air mole fraction of CFC (Figure 3), k_i is the gas transfer rate (centimeters per hour) used in the i th experiment, R is the fraction of sea ice cover (Figure 6), k_o is a constant, u is wind speed, and Sc is the Schmidt number for CFC-11 or CFC-12.

and, subsequently, the renewal of Antarctic Intermediate Water in the model ocean [England *et al.*, 1993]. In the transient tracer simulations this process is traced nicely by CFC-tagged waters that are first convected vertically in the southeast Pacific Ocean and then redistributed horizontally at intermediate levels. In the northern hemisphere, virtually no surface convective events are detected during July to October. Again, it seems that even in polar waters the model ocean has a tendency to establish near-surface stratification during the summer months.

4. Including CFC Uptake in the Model

As mentioned above, we take as our control experiment the simulation obtained when our ocean domain is subjected to an unadjusted, seasonally varying thermohaline and wind stress forcing (derived from the standard climatological data sets). This control run is then used to examine the sensitivity of the CFC simulation to a range of air–sea gas exchange parameterizations (see Table 1). The forcing of CFCs in the ocean model is varied because we want to gauge the relative sensitivity of the CFC simulation to the prescribed air–sea flux of gases. To run a simulation of CFC uptake, we take the equilibrated ocean circulation model (typically derived from a 3000 to 4000 year integration) and restart the integration with two additional tracers (CFC-11 and CFC-12), initially at zero concentration everywhere. The model is then run nominally from year 1930 until the end of 1988 with an uptake of the atmospheric gases CFC-11 and CFC-12. The industrial release of these gases began in the early 1930s and accelerated greatly during the next three decades (Figure 3). Even though virtually all production and release of CFCs has occurred in the northern hemisphere, rapid mixing rates in the lower atmosphere and the chemical stability of CFCs ensure relatively uniform distributions of these gases over the troposphere. In fact, the latitudinal variation of atmospheric CFC concentration is small enough [Cunnold *et al.*, 1983a, b] to take the distribution to be a simple function of hemisphere and time. Effectively, southern hemisphere concentrations lag the northern hemisphere values by just over 1 year [Warner and Weiss, 1992]. Figure 3 shows the estimated concentration of atmospheric CFC-11 and CFC-12 in the southern and northern hemispheres during this century (details of the derivation of these estimates are given by Warner and Weiss [1992] and Doney and Bullister [1992]). To give the model ocean a surface source term for atmospheric CFC entry, we need to consider the solubility of CCl_3F (CFC-11) and CCl_2F_2 (CFC-12) in seawater, which has been derived experimentally by Warner and Weiss

[1985]. In moist air and at a given pressure (assumed to be constant at 1 atmosphere) the solubility of CFC-11 and CFC-12 varies as a function of temperature and salinity, though in seawater the temperature dependence greatly outweighs the influence of salinity. The solubility varies inversely with temperature (e.g., water at 0°C can dissolve about four times more CFC-11 than water at 26°C), giving the CFCs a greater signature at high latitudes. This enhances the potential for CFCs to act as tracers of the deep and

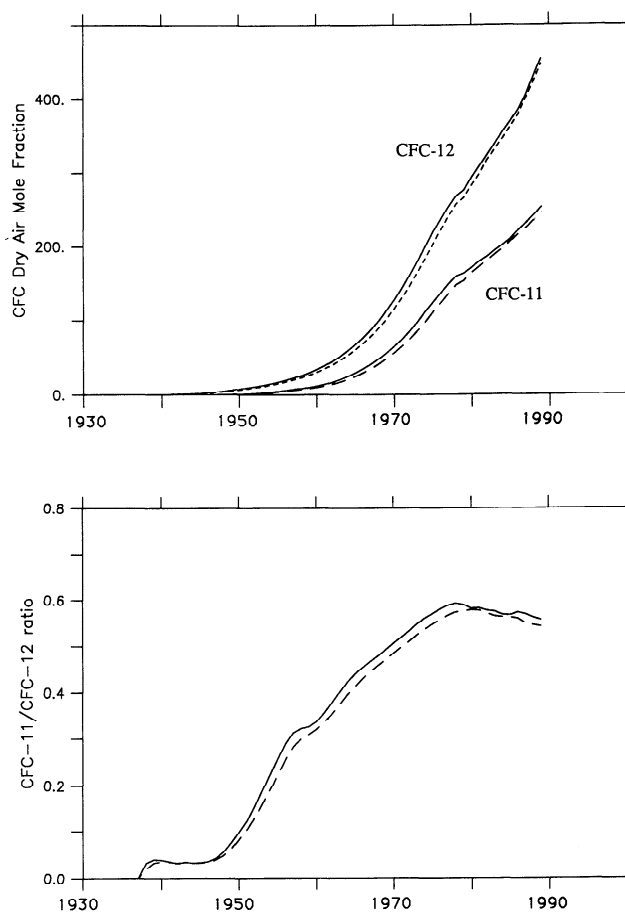


Figure 3. Reconstructed history of (top) the atmospheric dry air mole fractions of chlorofluorocarbons (CFCs) CFC-11 and CFC-12 and (bottom) their ratio (CFC-11/CFC-12). The solid lines correspond with values estimated for the northern hemisphere, with values in the southern hemisphere dashed. In effect, the southern hemisphere concentrations lag the northern hemisphere values by just over 1 year.

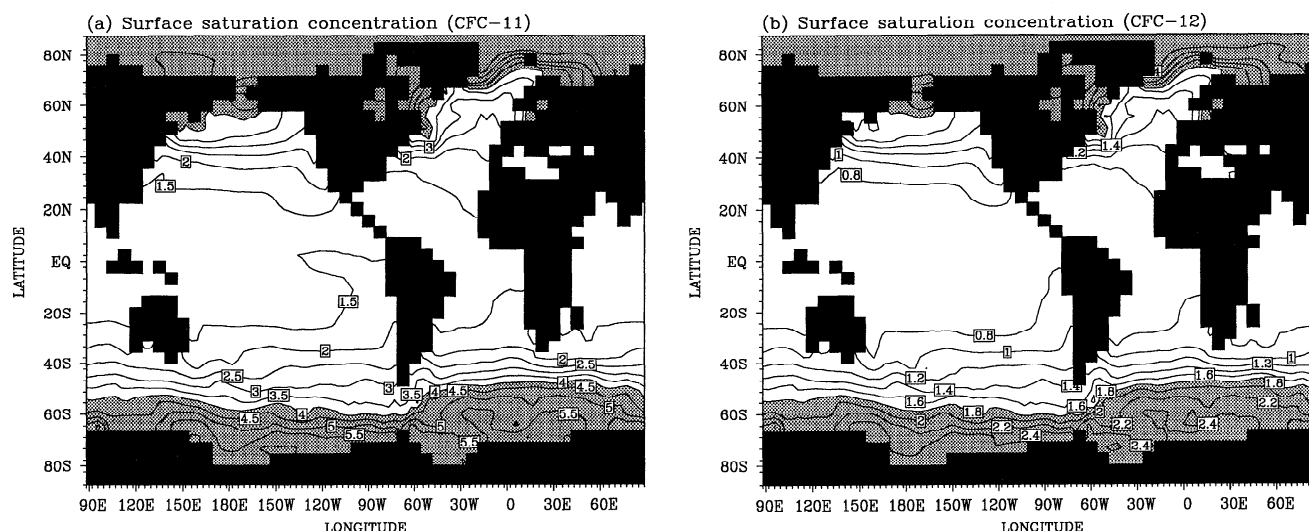


Figure 4. Surface seawater equilibrium (or saturation) concentrations of (a) CFC-11 and (b) CFC-12 during 1984, calculated using the solubility equations of Warner and Weiss [1985]. Units are picomoles per kilogram. Regions of CFC-11 concentration greater than 4 pmol/kg and CFC-12 concentration greater than 1.8 pmol/kg are stippled.

bottom water circulation over the 20- to 30-year timescale, as the solubility property favors a high signal to noise ratio in polar and subpolar waters.

We use our model ocean surface T and S fields to compute the oceanic concentration of CFC-11 and CFC-12 that would exist under equilibrium conditions (i.e., were the ocean 100% saturated with CCl_3F and CCl_2F_2). Because the ocean model varies seasonally, these saturation levels will vary with a cycle that tracks seasonal oscillations in sea surface temperature. Maps of the annual mean equilibrium ocean concentration of CFC-11 and CFC-12 during 1984 are shown in Figure 4. These maps are simply the atmospheric concentration observed during 1984 (approximated by our two-hemisphere distribution and interpolated to a set of monthly means) multiplied by the Warner and Weiss [1985] solubility constants. Although atmospheric CFC-12 concentrations are almost double those of CFC-11 (Figure 3), the greater solubility of CFC-11 in seawater yields much higher saturation concentrations for this compound. Because of the strong dependence of CFC solubility on temperature, Figure 4 also reveals the location of unusually cold or warm ocean temperatures at given latitudes. For example, the influence of the Gulf Stream and the NADW conveyor can be seen in the far North Atlantic, with greatly reduced CFC saturation concentrations compared with the cooler North Pacific. In the tropical Pacific, CFC-11 concentrations vary by as much as 25%; surface waters can dissolve more CFC in the cooler east Pacific than in the western Pacific warm pool.

Saturated Surface Experiment (Experiment CF1)

The saturation concentrations of CCl_3F and CCl_2F_2 in seawater (which vary interannually due to the release histories and intra-annually due to seasonal changes in T and S) are the basis for the four CFC forcing sensitivity experiments described here. In the first such experiment (CF1) we simply set the surface level concentration of CFCs to the saturation value, namely

$$\text{CFC}_w(x, y, t) = \alpha_c(\theta, S)\text{CFC}_{\text{atm}}(y, t) \quad (1)$$

where CFC_w is the model surface ocean concentration of CFC-11 or CFC-12, x, y are the standard horizontal coordinates, \pm is time, α_c is the CFC solubility reported by Warner and Weiss [1985] as a function of temperature θ and salinity (S), and CFC_{atm} is the atmospheric dry air mole fraction of CFC-11 or CFC-12 (drawn in Figure 3). As has been mentioned, the latitudinal variations in CFC_{atm} are approximated by an assumption of homogeneity within hemispheres.

The surface forcing in run CF1 is an oversimplification that favors strong ocean uptake of CFCs, since the ocean tends to be undersaturated in polar waters and in regions of upwelling [e.g., Wallace and Lazier, 1988; Doney and Bullister, 1992]. While the gas exchange will compete with the ocean circulation by trying to maintain the surface CFC concentrations at saturation or near-saturation levels, some balance will be achieved between the atmospheric forcing and the ocean circulation. The stronger the upwelling or convection, the more undersaturated the surface waters will be. In effect, the forcing in CF1 completely neglects the influence of the ocean circulation on the surface CFC concentrations. In the model formulation, ensuring surface saturation even requires suppressing the advection, diffusion, and convection terms in the surface tracer equations for CFC-11 and CFC-12.

Constant Gas Transfer Velocity Experiment (Experiment CF2)

The physical law governing air-sea gas exchange can be written [Liss and Merlivat, 1986; Wanninkhof, 1992]

$$Q = k(\alpha C_{\text{atm}} - C_w) \quad (2)$$

where Q is the gas flux across the air-sea interface (fluxes from the atmosphere into the ocean are positive), k is the gas transfer speed, C_w is the concentration of the given gas in the near-surface seawater, α is the solubility coefficient, and C_{atm} is the atmospheric concentration of the gas over the sea surface. For a given gas whose near-surface seawater and atmospheric concentrations are known and whose solubility

properties are understood, calculating the gas flux simply requires a parameterization of the gas transfer velocity k .

Using the notation defined previously, we can rewrite (2) for the gases CFC-11 and CFC-12 as

$$Q_c = k_c [\alpha_c(\theta, S) \text{CFC}_{\text{atm}}(y, t) - \text{CFC}_w(x, y, t)] \quad (3)$$

$$Q_c = k_c [\text{CFC}_{\text{eqm}}(x, y, t) - \text{CFC}_w(x, y, t)] \quad (4)$$

where Q_c is the flux of CFC-11 or CFC-12 into the ocean, k_c is the gas transfer velocity for CFC-11 or CFC-12, and CFC_{eqm} is the saturation concentration of the CFC as a function of space and time.

There are certain fundamental differences between the forcing of experiment CF1 and the forcing implied by (4). In experiment CF1 the surface forcing sets the upper level concentration, irrespective of local circulation conditions. Using (4), the CFC forcing enters the tracer equations as a source/sink term. This means that surface level concentrations are free to vary from saturated equilibrium levels. Indeed, the surface CFC concentrations will be influenced (like real ocean tracers) by advective, diffusive, and convective processes. The air-sea CFC fluxes will be generally positive because of the gradual increase in atmospheric CFC concentrations over the last half century. However, on certain occasions the ocean stores a slight excess of CFC-11 and CFC-12 (i.e., it is supersaturated). This can occur, for example, during summer months when the temperature-dependent CFC solubility decreases from its former winter-time high. On these occasions, the (4) parameterization would estimate a weak flux of CFC-11 and CFC-12 out of the ocean.

Several researchers have suggested bulk wind speed dependent parameterizations for the gas transfer velocities of certain gases [e.g., *Liss and Merlivat, 1986; Wanninkhof, 1992*]. In the final experiment of this study (experiment CF4) we adopt a complete parameterization (appropriate for climatological wind data) suggested recently by *Wanninkhof [1992]*. For the present experiment (experiment CF2), however, we adopt a constant gas transfer velocity k_2 over the entire model domain. The gas transfer speed chosen for both CFC-11 and CFC-12 is $k_2 = 10.6 \text{ cm/h}$, yielding an effective surface level equilibration timescale γ of

$$\gamma = \Delta z_1 / k_2 \approx 20 \text{ days} \quad (5)$$

where Δz_1 is the depth of the uppermost model level (50.9 m). The CFC gas transfer velocity was chosen as such for two reasons. First, this is an approximate mean value for wind speed conditions observed over the global ocean (see Figure 7). Secondly, it yields an equilibration timescale (or residence time) that is typical for a 50-m deep mixed layer [e.g., *Doney and Bullister, 1992*], reflecting the relatively rapid exchange (a few weeks [*Broecker and Peng, 1982*]) of these simple gases in the upper ocean.

The resulting saturation percentages found in experiment CF2 are drawn in Figure 5a. The map actually corresponds with the annual mean saturation percentage simulated during 1984. The distribution shown in this figure is typical of most of the CFC integration, since areas of undersaturation are directly related to the already equilibrated circulation field. By the late 1950s the upper CFC concentrations have already established a pattern that keeps the saturation variability more a function of ocean circulation than time. Areas of undersaturation are mostly linked with the regions of deep

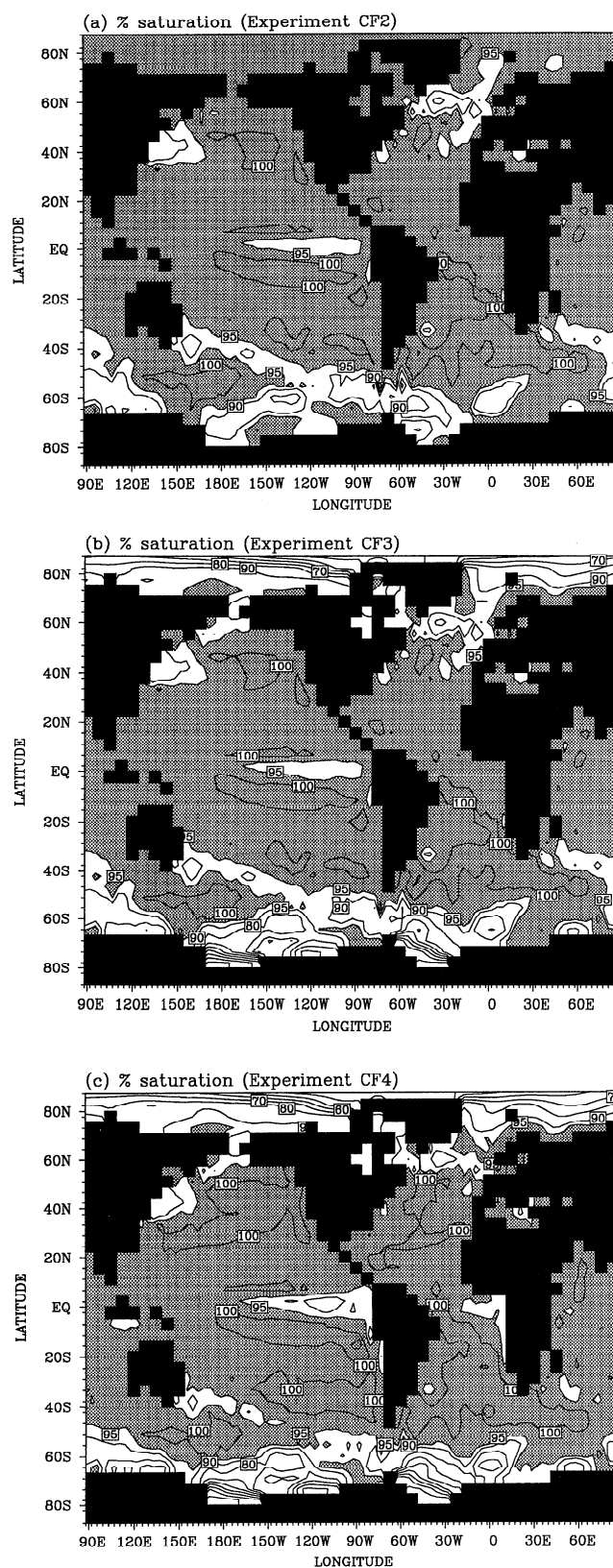


Figure 5. Annually averaged percentage of saturation (during 1984) simulated in the three experiments where surface CFC concentrations are permitted to deviate from saturated equilibrium, (a) experiment CF2, (b) experiment CF3, and (c) experiment CF4. Regions where the surface CFC concentrations are more than 95% of the saturated equilibrium are stippled. Contours are drawn at 10% intervals, with extra levels shown at 95% and 105% of saturated equilibrium.

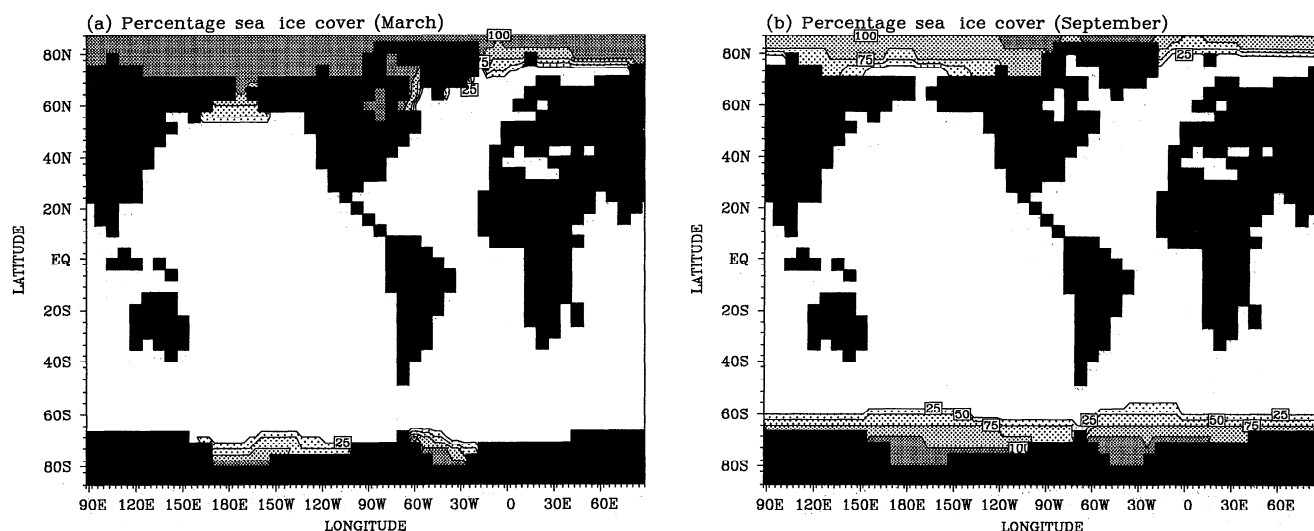


Figure 6. Climatologically derived percentage cover of sea ice used to parameterize limited air-sea gas exchange in polar ice-covered waters during (a) March and (b) September. A smooth sinusoidal interpolation between these extreme cases defines the sea ice coverage during the rest of the year.

convection in the model (e.g., see Figure 2). Annual mean undersaturation is as high as 20% in some areas of the Southern Ocean and in the far North Atlantic. Of course, with a marked seasonal cycle in surface temperature and surface convective intensity (Figure 2) there is also a seasonal cycle in CFC saturation levels. In regions with an annual mean saturation level of 80% the typical wintertime CFC concentration can be as low as 50% saturation (with near-saturation levels for most of the rest of the year). Maximum undersaturation is reached during the height of a wintertime convective event. More typical convective layer undersaturations are in the range 10–35% (realized during winter over the unshaded high-latitude regions of Figure 5a). This is in quite good agreement with observed levels of surface CFC concentrations over convected waters (e.g., ~40% undersaturation in newly formed LSW [Wallace and Lazier, 1988], ~25% undersaturation in the Norwegian-Greenland sea [Bullister and Weiss, 1983]).

Other prominent regions of undersaturation appear where the ocean model upwells, for example, in the tropical eastern Pacific and in the western boundary currents. The level of undersaturation in the equatorial mixed layer is in the range 3–8%, in good agreement with field observations (e.g., Doney and Bullister [1992] quote 4–6% undersaturation in the equatorial Atlantic during August 1988). This demonstrates that the experiment CF2 flux condition is correctly allowing even subtle levels of undersaturation to develop in response to the ocean circulation. Between 30°S and 30°N (but outside the equatorial upwelling belt) there are some regions where the ocean is supersaturated (by 1–4%) with CFC-11 and CFC-12. This is due to seasonal oscillations in temperature; during summer the atmosphere warms previously cool waters to temperatures that have somewhat lower equilibrium concentrations than the cool winter water. If the temperature cycle is strong enough, then supersaturated CFC water will appear in the summer mixed layer. Measurements of ~4% supersaturated CFC waters were noted at low- to midlatitudes in the Atlantic Ocean during summer 1988 [Doney and Bullister, 1992].

Fractional Air-Sea Gas Exchange Over Ice-Covered Regions (Experiment CF3)

In our estimations of CFC fluxes into the ocean in experiments CF1 and CF2 we have neglected the influence of sea ice in limiting the area of ocean exposure to the atmosphere. In run CF3 we make some attempt at incorporating this process into our parameterized CFC forcing. Estimations of sea ice coverage have been digitized from several recent analyses of satellite-derived sea ice cover in the Arctic Ocean [Parkinson *et al.*, 1987] and around the Antarctic continent [Comiso *et al.*, 1993]. These ice cover functions are drawn for the months of March and September in Figure 6. The chosen months represent, respectively, the maximum northern hemisphere and southern hemisphere winter coverages. A smooth sinusoidal interpolation between these two cases defines the monthly sea ice coverage masking the ocean-atmosphere gas exchange in the model. The CFC flux parameterization used in CF3 is exactly that used in experiment CF2, only the fluxes are limited in direct proportion to the monthly sea ice coverage. In effect, the CF3 gas transfer velocity k_3 is calculated according to the relation

$$k_3 = k_2(1 - R) \quad (6)$$

where R is the fraction of sea ice cover in our approximated climatology and k_2 , k_3 are the gas transfer speeds used, respectively, in experiments CF2 and CF3. Evidently, the CF3 transfer rate lies between 0 cm/h (total ice cover) and k_2 cm/h (no sea ice). Total ice cover shuts down the air-sea CFC exchange in the height of winter in the Arctic Ocean and in parts of the Ross and Weddell Seas (Figure 6). Correspondingly, surface saturation levels become greatly reduced in these polar waters (Figure 5b). Minimum surface CFC concentrations in regions of persistent ice cover reach as low as 75% undersaturation during winter (i.e., only 25% of saturation equilibrium). This may, at first, seem an exaggeration of the influence of sea ice cover in the model, though it should be noted that observational studies suggest similar figures. For example, Schlosser *et al.* [1991] found

CFC-11 concentrations in newly formed Weddell Sea Bottom Water (WSBW) that suggest the water was at about 35% of saturated equilibrium at the time of formation. Even weaker levels of saturation might be found in persistently covered sea ice regions.

Wind Speed Dependent Gas Transfer Experiment (Experiment CF4)

In the last of our four sensitivity experiments we adopt a gas transfer rate that depends on the local sea ice cover R and wind speed u , as well as the kinematic viscosity of seawater μ and the diffusion coefficient D of CFC-11 and CFC-12. The dependence of k_c on the latter two terms is normally expressed using the Schmidt number Sc , where $Sc = \mu/D$. Wanninkhof [1992] fits polynomial approximations to Sc for a range of environmental gases, including CFC-11 and CFC-12. The value of Sc varies inversely with temperature; that is, cooler waters have higher Schmidt numbers. However, it is well known that over the ocean the local wind speed has a greater role in determining gas transfer rates.

In experiment CF4 the formulation of Wanninkhof [1992] is chosen, in particular because he gives a parameterization appropriate for climatological wind speed data (such as that of Esbenson and Kushnir [1981]). Taking into account possible chemical enhancement effects at low wind speeds and the time variability of surface winds, he suggests that for a steady wind field (such as a seasonally varying climatology)

$$k = k_o u^2 / (Sc)^{1/2} \quad (7)$$

where k_o is a constant (7.964) derived from bomb-produced radiocarbon invasion rates into the ocean (which includes implicitly the Schmidt number for ^{14}C), u is the climatological wind speed (in meters per second), and Sc the Schmidt number for a given gas. Differences between the Schmidt numbers for CFC-11 and CFC-12 yield air-sea gas transfer rates that are 4–7% faster for CFC-12. The gas transfer rate in experiment CF4 k_4 can then be written

$$k_4 = k_o u^2 (1 - R) / (Sc)^{1/2}. \quad (8)$$

In the calculation of k_4 , we reference the Esbenson and Kushnir [1981] seasonally varying wind speeds and compute Sc as a function of model temperature for each gas. That is, k_4 varies seasonally on account of seasonal changes in the surface wind speed, upper level temperature, and sea ice cover.

Computed values of k_4 can be directly compared with the CF2 assumption that k_c is constant at 10.6 cm/h. Figure 7 shows maps of the annual mean gas transfer speed for CFC-11 and CFC-12 before the sea ice effect is factored into the parameterization. The separation of sea ice effects from the wind speed dependence is useful for examining the specific influence of the Wanninkhof [1992] relation in experiment CF4. Also included in Figure 7, for easy reference, is the annual mean wind speed climatology of Esbenson and Kushnir [1981]. Calculated gas transfer speeds vary about the CF2 benchmark of 10.6 cm/h; under the subpolar westerlies in the Southern Ocean the gas piston velocity is persistently faster than 12 cm/h, whereas slower exchange rates are estimated over much of the tropical and high-latitude waters. The corresponding

surface level equilibration timescale (Figures 7d and 7e) varies between 12–20 days (in the subpolar wind belts) and 40–70 days in the western equatorial Pacific and in the Ross and Weddell Seas. The slightly faster CFC-12 transfer rates are evident in Figure 7c.

The percentage level of surface CFC saturation is drawn for CFC-11 in Figure 5c. Over much of the ocean the Wanninkhof [1992] parameterization yields similar upper level CFC concentrations as the $\gamma = 20$ days assumption of experiments CF2 and CF3. However, weaker surface gas fluxes are estimated at high latitudes and in the tropics (note, for example, the appearance of more waters of sub-95% saturation along the equatorial waveguide). In contrast, more CFC uptake is simulated under the subpolar wind belts, with certain convectively active regions now maintaining near-saturation levels on the annual mean.

5. CFC Simulations in the World Ocean Model

In terms of our CFC simulations, the convective regions indicate those parts of the deeper ocean that become directly exposed to atmospheric conditions. As such, we can expect significant traces of CFC-11 and CFC-12 at depth in the Southern and North Atlantic Oceans. To present an overview of the CFC simulations, Tables 2a, 2b, and 2c include some values for the maximum simulated concentrations in certain key areas of the model domain. Since we have chosen to focus our attention on the deep and bottom water ventilation, most of the chosen areas correspond to model regions of deepwater formation or bottom water flow off the Antarctic shelf. Many of the sampling locations and times were also chosen to correspond with available measurements of real ocean CFC-11 concentration.

CFC-11 Simulations in the Deep Southern Ocean

The concentration of CFC-11 at model levels 10 and 11 (2935-m and 3721-m depth) is shown for a zoom in the southern hemisphere during late 1983 in Figure 8. Each of the four experiments reproduces the northward propagation of AABW in the Atlantic sector of the model, with a subtle reduction in CFC extension as the surface gas transfer rate becomes more realistic (e.g., note the northward extent of the 0.015-pmol/kg contour). The Atlantic traces of bottom water also propagate eastward into the south Indian Ocean. In the Pacific Ocean, bottom waters formed in the Ross Sea overflow into the Southwest and Southeast Pacific Basins. The extent of northward spreading in the Pacific Ocean is somewhat weaker than that in the Atlantic Ocean. This is because deep ocean currents are weaker in the Ross Sea outflow compared with those that spread from the WSBW formation zone.

It is a little difficult to visualize the significant variations in deep Southern Ocean CFC-11 concentrations shown in Figure 8. To emphasize the different concentrations obtained with each change in surface CFC forcing, the reader is directed to certain model water samples taken from the four simulations (Table 2a). For example, water convectively overturned in the Weddell Sea near 4000 m depth is far too enriched with CFC-11 in runs CF1 and CF2. Reasonable concentrations are simulated once the proportion of sea ice cover is factored into the gas exchange timescale. Ross Sea Bottom Water (RSBW) also follows a trend of reduced CFC-11 concentrations as the surface gas forcing improves.

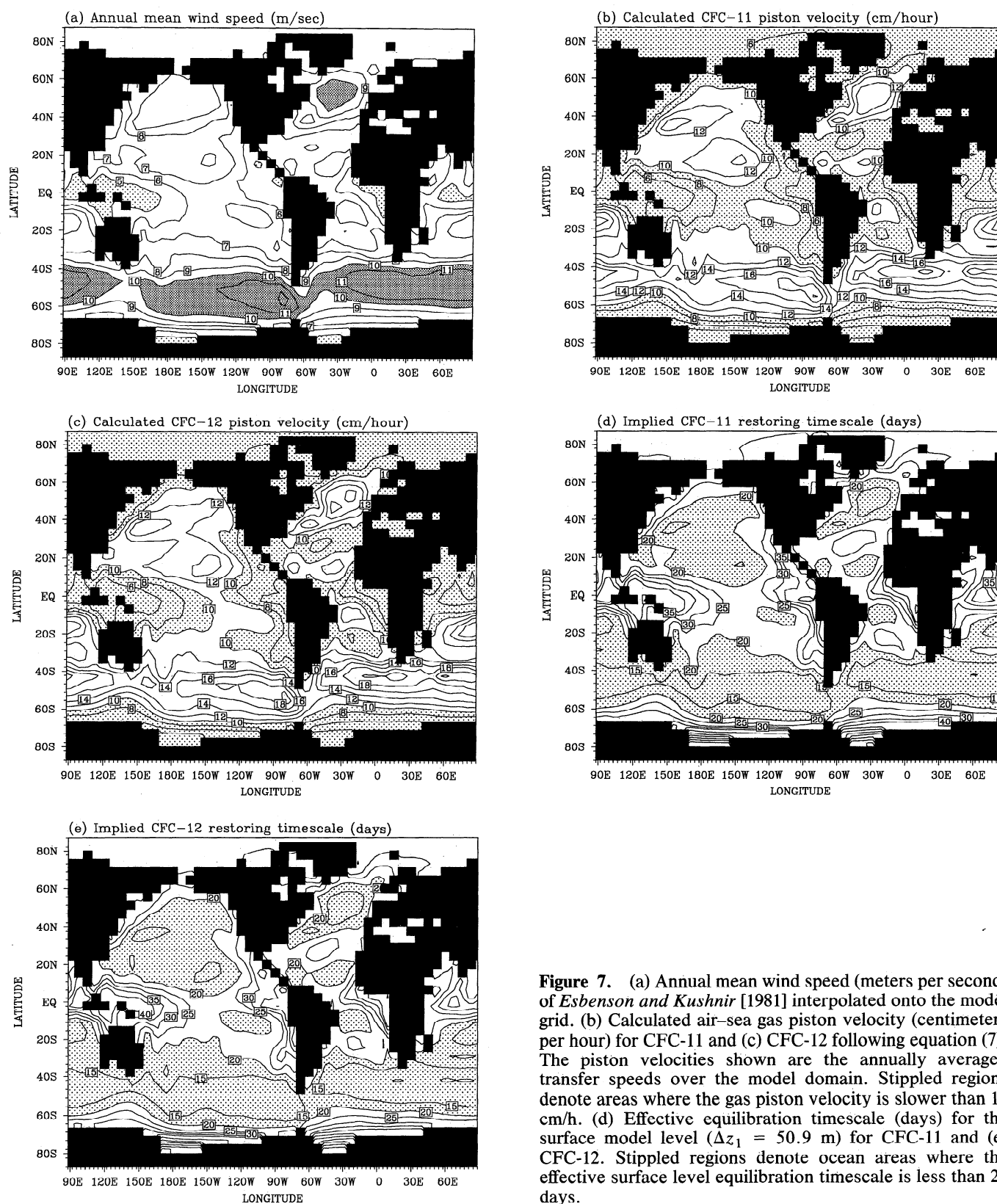


Figure 7. (a) Annual mean wind speed (meters per second) of *Esbenson and Kushnir* [1981] interpolated onto the model grid. (b) Calculated air-sea gas piston velocity (centimeters per hour) for CFC-11 and (c) CFC-12 following equation (7). The piston velocities shown are the annually averaged transfer speeds over the model domain. Stippled regions denote areas where the gas piston velocity is slower than 10 cm/h. (d) Effective equilibration timescale (days) for the surface model level ($\Delta z_1 = 50.9$ m) for CFC-11 and (e) CFC-12. Stippled regions denote ocean areas where the effective surface level equilibration timescale is less than 20 days.

Table 2a. Maximum CFC-11 Concentrations in Southern Ocean Bottom Water

Experiment	WSBW, 3721 m	RSBW, 2935 m	Ajax Section	SAVE leg 3
CF1	4.63	4.25	3.05	0.292
CF2	3.15	2.63	1.65	0.165
CF3	1.72	1.52	1.33	0.086
CF4	1.62	1.40	1.26	0.078
Observed	1.65	...	0.28	0.034

Specific levels and years were chosen to match particular cruise data that have been published. These data are included for easy reference and intercomparison between the CFC simulations. All values are in picomoles per kilogram. The Weddell Sea Bottom Water (WSBW) and Ross Sea Bottom Water (RSBW) concentrations are sampled during model year 1987 just off the shelf outflow around the Antarctic continent. The "Ajax section" data correspond with the bottom water simulated along the prime meridian during the model period October 1983 to January 1984. The South Atlantic Ventilation Experiment "SAVE leg 3" data are the maximum bottom water traces of CFC-11 found off the western boundary near 25°S during March 1988. The model samples of bottom water in the Weddell Sea, at the Ajax section, and near 25°S can be compared directly with data obtained during hydrographic surveys (taken from Schlosser *et al.* [1991], Warner and Weiss [1992], and Weiss *et al.* [1993]).

These variations in bottom water CFC concentrations can be seen in the southernmost regions shown in Figure 8, with a progressive shrinking of the CFC extensions as higher surface undersaturations are simulated.

Measured CFC-11 concentrations along some of the South Atlantic Ventilation Experiment (SAVE) sections confirm the presence of CFC-enriched waters along the bottom western boundary of the South Atlantic Ocean. Concentrations as high as 0.034 pmol/kg were found near 4200 m depth near 25°S during March 1988 [Weiss *et al.*, 1993]. These relatively high traces of CFC-11 can be traced directly to an Antarctic origin. The model simulates the bottom water ventilation of the Atlantic Ocean too strongly. For example, note the northward extension of the 0.03-pmol/kg contour in the four experiments during late 1983 (Figure 8), around 4 years earlier than when the SAVE leg 3 measurements were made. The 0.03-pmol/kg signal in 1983 is as far north as 10°S (experiment CF1), even though the sections presented predate the SAVE cruise time by 4 years. Even in experiment CF4, the 0.03-pmol/kg signal reaches the SAVE leg 3 latitude (25°S)

around 4 years too early (Figure 8d). A direct comparison between the SAVE leg 3 data and the model simulations (Table 2a) reveals the degree of sensitivity of the deep CFC simulations to the surface gas forcing used, and how the experiments with high polar undersaturation (CF3 and CF4) give the best representation of the northward propagating CFC signal. However, in all four experiments the propagating signal overshoots the observations in the bottom water outflow zones, even when concentrations are realistic in the original formation regions (Table 2a). It should also be noted that with the coarse vertical resolution at depth, unrealistically thick layers of CFC-tagged bottom water are simulated in the northward extensions into the Atlantic, Indian, and Pacific Oceans.

Modeled and observed CFC-11 concentrations are shown along the Greenwich meridian during late 1983 in Figure 9. The observed section is redrafted from Warner and Weiss [1992] and corresponds with measurements made as part of the Ajax experiment during late 1983. Equatorward of around 45°S, the CFC simulations appear to reproduce the observed concentrations rather well, although the model concentrations are somewhat more diffused in the main thermocline. Marked differences between the model and observations appear in the extreme Southern Ocean. For example, note the location of the 1.6-pmol/kg contour south of 50°S; in the observed section it remains in the upper 300 m of the water column, whereas the CF1 model fills the entire water column south of the Southwest Indian Ridge with water whose CFC-11 concentration exceeds 1.6 pmol/kg. This can be seen in Figure 8a with the eastward spreading of the 1.6-pmol/kg contour across the prime meridian at 3721 m depth in experiment CF1. Marked improvement is made as the surface waters become CFC undersaturated, with the CF3 and CF4 simulations clearly superior. Maximum sampled bottom water CFC-11 concentration along the prime meridian is 0.28 pmol/kg in the observed data, whereas it exceeds 3.0 pmol/kg in run CF1 (Table 2a). This discrepancy amounts to an order of magnitude error in deep CFC-11 concentrations in the "saturated surface" run. Even in runs CF3 and CF4, the deep CFC-11 concentrations are too high by a factor of about 4. This suggests that not enough older (CFC-deprived) water recirculates and upwells into the Southern Ocean. For example, more upwelled circumpolar deep water in the Southern Ocean would weaken the CFC-11 concentrations significantly, not only because the older water would contribute to a lower CFC mixture, but also

Table 2b. Maximum CFC-11 Concentrations in North Atlantic Deep Water (NADW) Sources and Outflow

Experiment	LSW, 295 m	LSW, 2228 m	NADW _{outflow}
CF1	4.18	3.39	0.008
CF2	3.51	2.66	0.005
CF3	3.41	2.63	0.005
CF4	3.33	2.67	0.006
Observed	3.05	1.85	0.050

Values are in picomoles per kilogram. The Labrador Sea Water (LSW) is shown for the upper convective mixed layer during the model winter of 1986 (for comparison with the observations of Wallace and Lazier [1988]) and for the deeper shelf overflow during July and August 1988 (for comparison with Doney and Bullister [1992]). The NADW outflow concentration is measured near the equator during December 1982 to February 1983 (to correspond with the observations of Weiss *et al.* [1985]).

Table 2c. Maximum CFC-11 Concentrations in Arctic Ocean Deep and Bottom Water

Experiment	NSO, 2228 m	CAOB, 1622 m	NB, 2935 m
CF1	1.32	0.123	0.061
CF2	1.07	0.097	0.050
CF3	0.96	0.081	0.041
CF4	0.92	0.077	0.038
Observed	...	0.010	0.010

The CFC-11 concentrations (in picomoles per kilogram) are shown for the Norwegian Sea overflow (NSO) of deep water during 1986 (near 0°, 70°N), in the deep Central Arctic Ocean Basin (CAOB) during 1983 (near 108°W, 85°N), and in the deep Nansen Basin (NB) during July–August 1987 (near 30°E, 84°N). The modeled concentrations in the Nansen and Central Arctic Ocean Basins can be compared directly with the observations of Krysell and Wallace [1988] and Wallace and Moore [1985].

(a) Experiment CF1

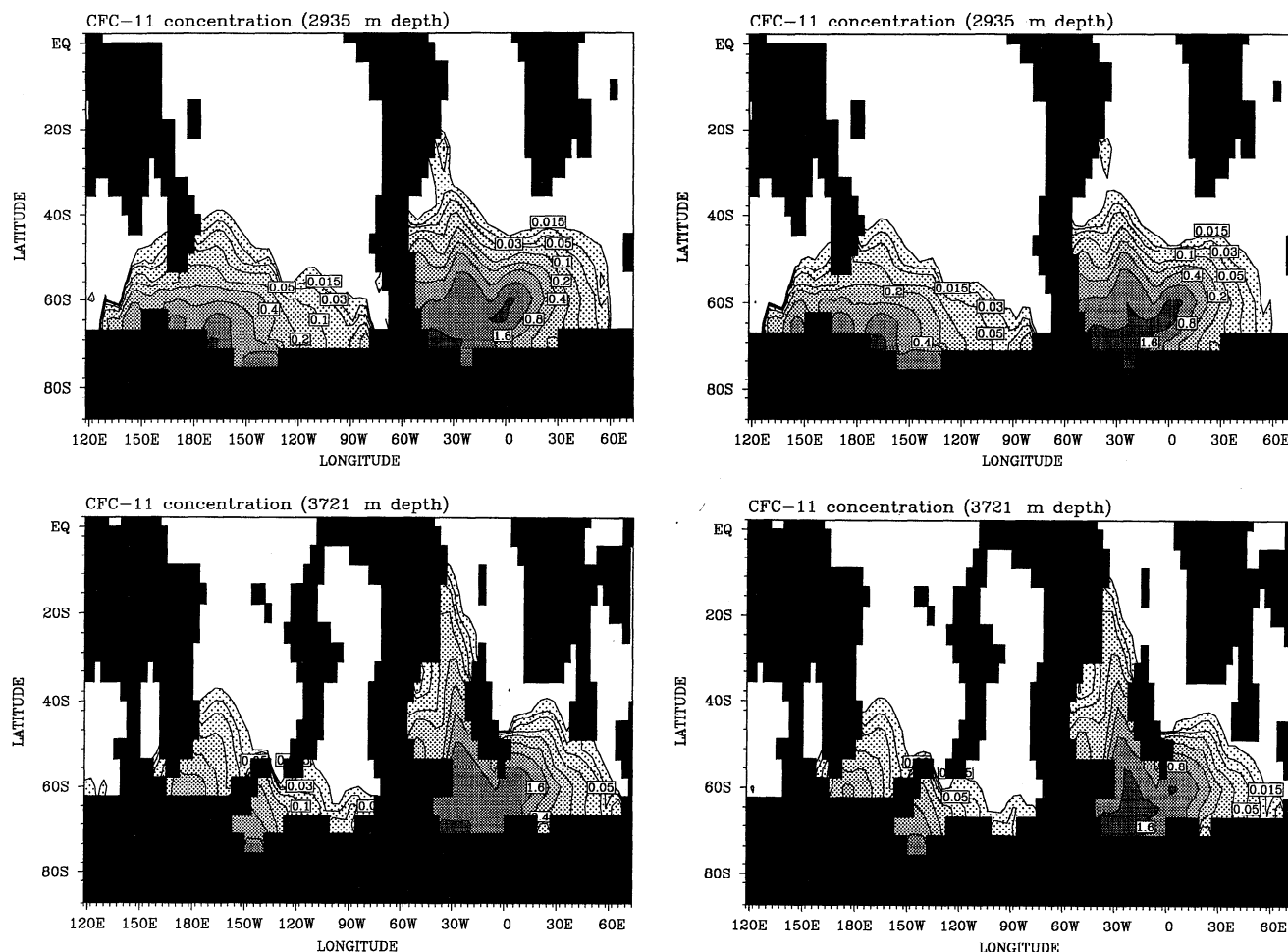


Figure 8. Concentration of dissolved CFC-11 at 2935-m and 3721-m depth (model levels 10 and 11) during late 1983 in runs (a) CF1, (b) CF2, (c) CF3, and (d) CF4. To be consistent with observational studies, we draw contour levels at 0.015, 0.03, 0.05, 0.1, 0.2, 0.4, 0.8, 1.6, and 3.2 pmol/kg.

because the convective activity in the region would tend to be suppressed (see part 2).

To further illustrate the sensitivity of the modeled CFC uptake to changes in the air–sea gas exchange, we include the difference in Ajax section CFC-11 concentrations between the respective experiments in Figure 9. The reduction of upper level CFC concentrations over regions of deep convective overturn in run CF2 leads to a reduced CFC signature over much of the Southern Ocean. At the Ajax section the maximum surface difference is centered near 60°S, since this is precisely the latitude of maximum convective activity along the prime meridian (see Figure 2b). The change in CFC-11 concentration along the Ajax section in experiment CF3 indicates the effect of sea ice in reducing ocean uptake of atmospheric CFC over the extreme polar regions of the Southern Ocean. CFC concentrations in experiment CF3 are necessarily less than or equal to the CFC concentrations in experiment CF2, with the difference signal highest off the Antarctic shelf. The model ocean circulation redistributes this signal, with 0.01 pmol/kg CFC-11 concentration changes noted as far north as 40°S in the upper 1000 m and up to 50°S over the Southwest Indian

Ridge (Figure 9g). Including a wind speed dependent gas piston velocity in experiment CF4 enhances the CFC uptake in regions where this velocity is faster than 10.6 cm/h (the unshaded regions of Figure 9h). Broadly speaking, CFC fluxes are higher under the subpolar westerlies and in certain subtropical oceans and lower in the tropical and polar regions. The differenced Ajax section (Figure 9h) reveals these trends, with a significant reduction in CFC ventilation south of 60°S, contrasted with increased CFC uptake under the westerly wind belt (40°S–60°S). Differences of more than 0.1 pmol/kg are observed as deep as 1000 m, indicating the overall sensitivity of the CFC uptake to changes in the surface forcing.

CFC-11 Simulations in the Deep North Atlantic and Arctic Oceans

Maps of the concentration of CFC-11 at 1622 m depth in the North Atlantic Ocean are shown for each of the CF1–CF4 experiments in Figure 10. The CFC data are sampled from the model ocean during early 1983, in order to correspond with an equivalent diagram presented by Weiss *et al.* [1985]. The Weiss *et al.* [1985] diagram is derived from measure-

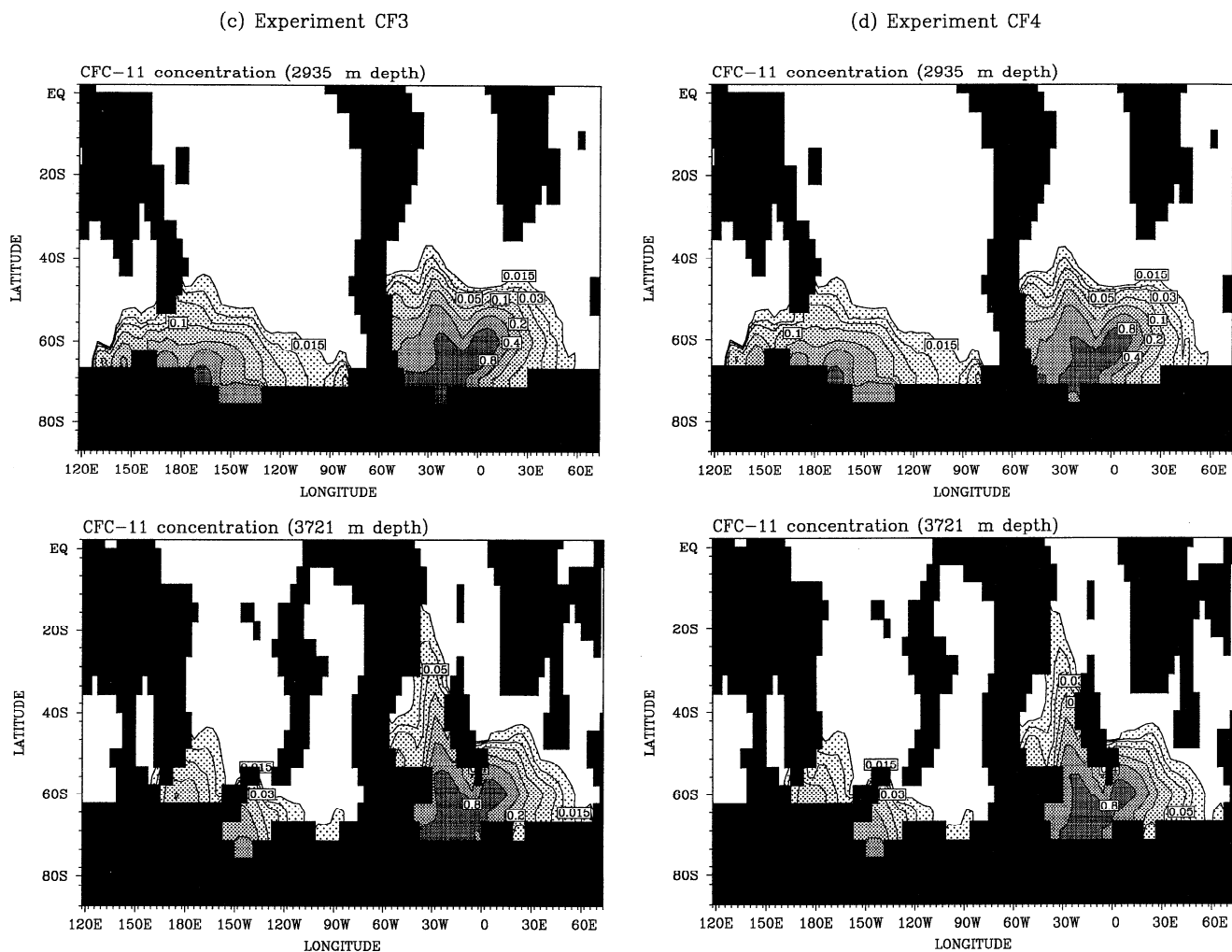


Figure 8. (continued)

ments made during the Transient Tracers in the Ocean (TTO) North Atlantic and tropical Atlantic studies. Because our model density field is free to vary from the observed ocean density structure, this map is best viewed on the level corresponding to maximum NADW outflow rates (i.e., level 8; see Figure 1b). Overall, the model reproduces the deep North Atlantic CFC-11 field quite well, except that concentrations in the western boundary outflow are far too weak (see also Table 2b). In effect, the model southward extension of the CFC-enriched upper NADW is not matching observations [see Weiss *et al.*, 1985]. This is because the model advective timescale limits the southward penetration of CFC-tagged waters during the transient uptake process (a run with zero horizontal diffusion acting on the CFC tracers confirms that the lateral diffusion in the model does not significantly erode the southward propagation of the CFC-enriched waters; see part 2). Outflow current speeds at 1622 m depth (Figure 11) are of the order of 1.5 cm/s (with some faster parts of the outflow reaching 2 cm/s). This is actually of the same order as the scale velocity of upper NADW outflow (originating in the Labrador Sea) derived by Weiss *et al.* [1985] (1.4 cm/s). What we see in the model simulation, however, is that much of the outflow of recently formed NADW

includes a loop eastward into the Northeastern Atlantic Basin. The extended path followed by the CFC-11 signature is thus around 14,000 km in distance (between the Labrador–Greenland Sea formation zone and the equator, Figure 11), somewhat greater than the 10,000 km distance assumed by Weiss *et al.* [1985]. In the model the CFC-tagged LSW therefore requires around 30 years to make its way to the tropical Atlantic (assuming a 1.5-cm/s mean speed). This timescale is confirmed by an age analysis of deep and bottom water in the model (Figure 12; see also part 2). On the basis of the value of the CFC-11/CFC-12 concentration ratio (compared with the atmospheric history of this ratio, Figure 3) we can estimate the age of water crossing the equator to be around 35 years. The CFC data typically overestimate the apparent age because of mixing between the CFC-tagged core and the adjacent waters [Pickart *et al.*, 1989]. The calculated model timescales for the outflowing NADW to cross the equator are somewhat longer than estimates derived from observed CFC distributions (e.g., Weiss *et al.* [1985] estimate 23 years). However, increasing the rate of outflow of NADW in the model can significantly reduce the age of deep water crossing the equator (see part 2), partly because the outflow waters opt for a shorter route to the tropics. As a consequence, younger

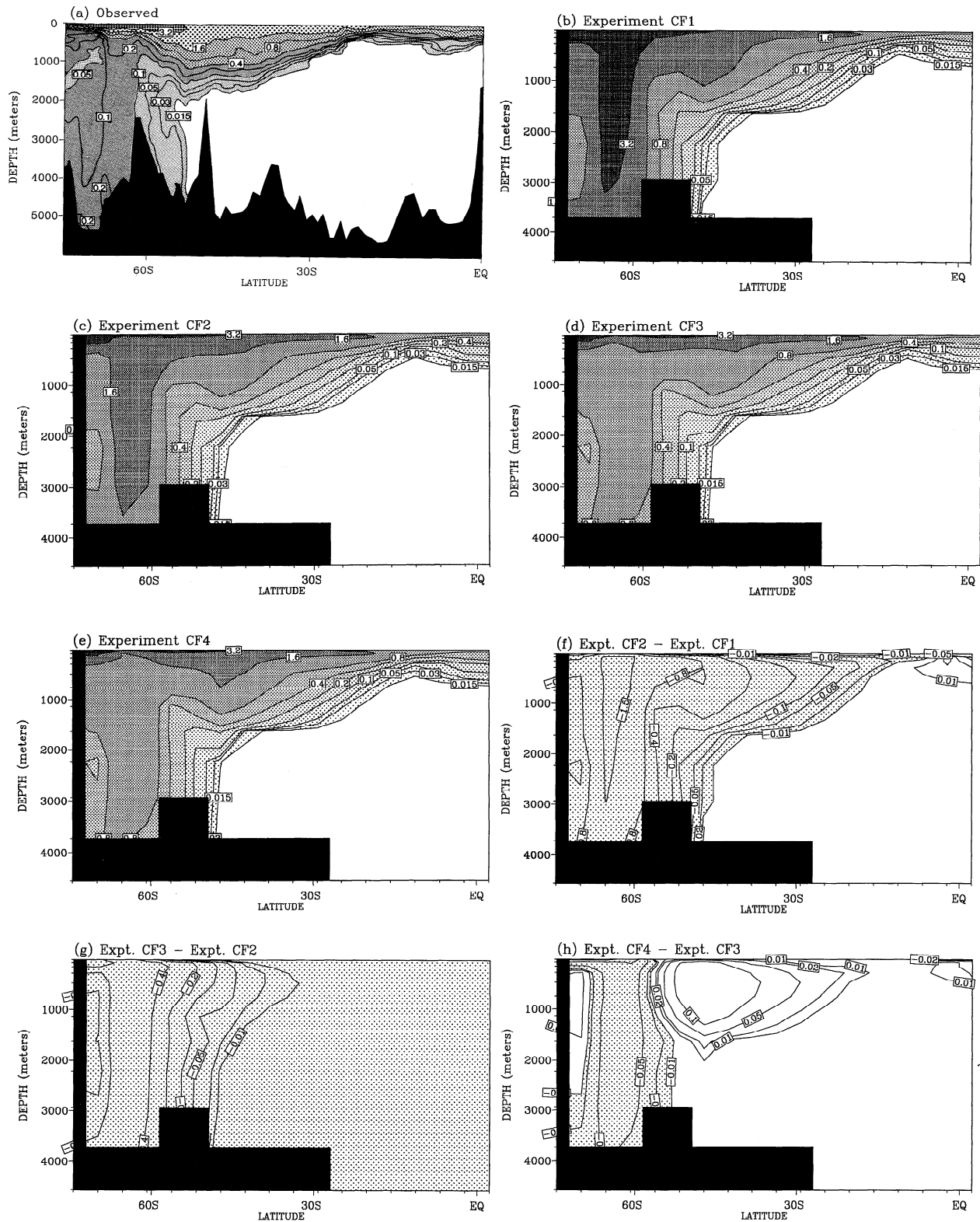


Figure 9. Latitude–depth sections of dissolved CFC-11 along the prime meridian during late 1983. (a) Observed (redrafted from Warner and Weiss [1992]). Distributions in runs (b) CF1, (c) CF2, (d) CF3, and (e) CF4. The contour levels chosen are the same as in Figure 8. Also shown are the differenced concentrations between (f) runs CF2 and CF1, (g) runs CF3 and CF2, and (h) runs CF4 and CF3. In the difference plots, contours are drawn at ± 0.01 , ± 0.02 , ± 0.05 , ± 0.1 , ± 0.2 , ± 0.4 , ± 0.8 , and ± 1.5 pmol/kg, and regions of negative difference are stippled.

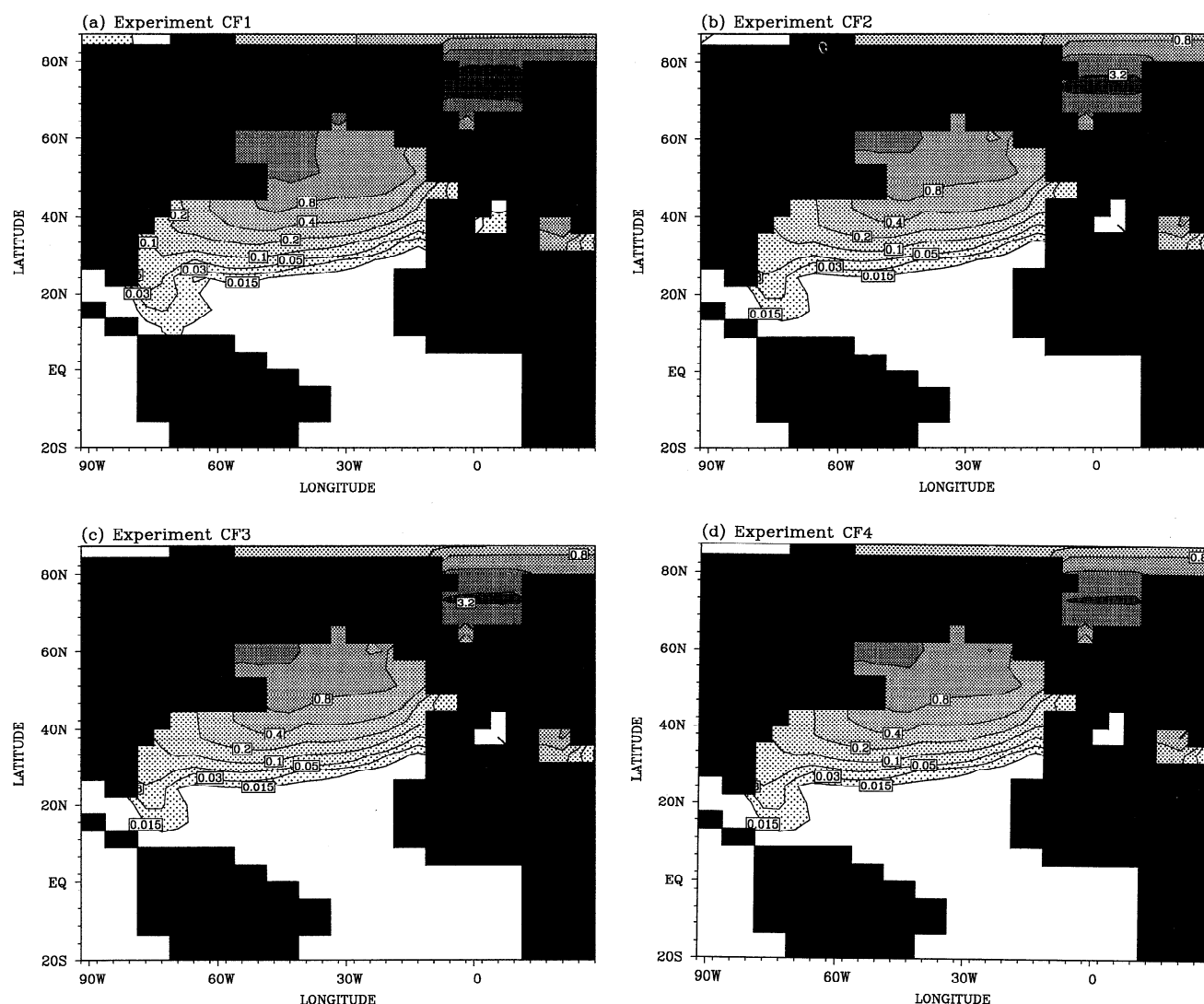


Figure 10. Concentration of dissolved CFC-11 at 1622 m depth (model level 8) during late 1982 in runs (a) CF1, (b) CF2, (c) CF3, and (d) CF4. Contour levels are drawn at the standard concentrations.

(CFC enriched) water spreads farther southward in such simulations.

The degree of dilution of a given water mass can also be calculated with the aid of CFC concentration data, if it is assumed that the water mass is diluted by surrounding waters that are essentially CFC free [e.g., Weiss *et al.*, 1985]. Such a calculation depends on the CFC concentration measured in the water mass compared with the concentration it originally had at the time of formation. This requires some knowledge of the degree of saturation of the surface water when the water mass was formed [e.g., Wallace and Lazier, 1988]. In ocean models we can sample surface saturation levels routinely, making the dilution calculation easy to perform. In our four control model CFC simulations the degree of dilution of NADW should be constant since the dilution processes are a function of the model circulation and mixing rates. The simplest approach is therefore to use run CF1 (since in this experiment, surface CFC concentrations are always in saturated equilibrium with the atmosphere). Water arriving at 10°N off South America is sampled during 1988 and found to have a CFC-11 concentration of 0.035 pmol/kg.

The age estimate for this water is around 32 years (Figure 12), meaning that it was originally exposed to the atmosphere in 1956. The historical data for CFC-11 in the northern hemisphere (Figure 3) shows an atmospheric dry air mole fraction of 5.69 in 1956, which for LSW ($\theta = 3.5^\circ\text{C}$, $S = 34.90\text{‰}$) yields an equilibrium concentration of 0.121 pmol/kg. That means the water arriving at 10°N (CFC-11 = 0.035 pmol/kg) has been ~70% (or 3.5-fold) diluted during its 32-year journey from the Labrador Sea mixed layer. The dilution is mostly caused by the vertical diffusion of the southward flowing CFC-enriched water along model level 8. Weiss *et al.* [1985] make a similar calculation derived from real ocean data, estimating upper NADW to be approximately 80% diluted by the time it arrives at the equator. However, their calculations incorrectly assumed the convective mixed layer to be in saturated equilibrium with the atmosphere. Wallace and Lazier [1988] suggest that Labrador Sea saturation levels might be typically 60% at the time of deepwater formation. This would bring the Weiss *et al.* [1985] estimate down to a threefold dilution by CFC-free waters.

Included in Tables 2b and 2c are certain key CFC-11

samples made during the model simulation in the North Atlantic and Arctic Oceans. The samples taken were chosen at locations and times that match observational records. In the convective region of the Labrador Sea in run CF1, CFC-11 concentrations are overestimated in the surface mixed layer and at depth. Improvements are made when a realistic timescale for upper layer equilibration is built into our air-sea gas model. In the NADW outflow region, marked deficiencies in CFC-11 concentration are modeled near the equator in all four runs. However, these low CFC levels can be mostly corrected with a change in the model outflow rate (part 2), even when the forcing of run CF4 is maintained. The concentration of CFC-11 in the deep Arctic Ocean is generally equal to or smaller than the minimum detectable level of 0.01 pmol/kg [e.g., Krysell and Wallace, 1988; Wallace and Moore, 1985]. Our simulations, in contrast, flux moderate levels of CFCs into the region (Table 2c). Once again, the overestimation of oceanic CFC uptake is reduced progressively during the model experimental sequence, with levels sampled in run CF4 somewhat closer to the observed data than the erroneous CF1 concentrations.

6. Discussion and Conclusions

The uptake and redistribution of anthropogenic CFC-11 and CFC-12 have been examined within a global ocean circulation model. In particular, model CFC simulations were generated using four different parameterizations of the air-sea gas exchange rate. The different CFC integrations were carefully sampled to generate model data sets that could be directly compared with certain observational studies of the concentration of CFC-11 in deep and bottom waters.

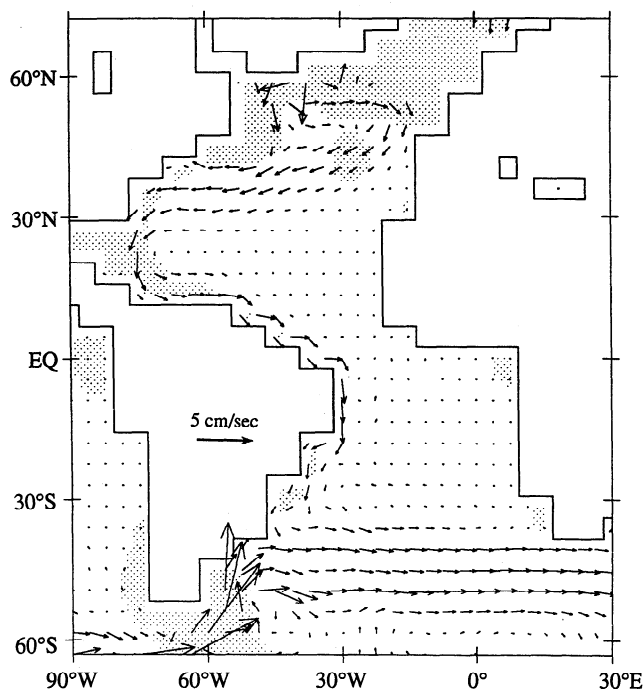


Figure 11. Ocean current vectors at 1622-m depth in the control ocean model. The vector scaling is indicated in centimeters per second. Subsurface topographic features at 3000 m depth (model level 10) or shallower are stippled.

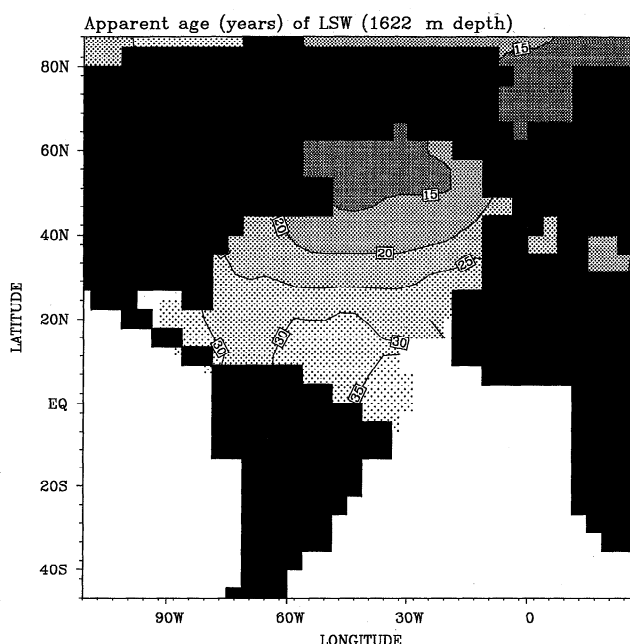


Figure 12. Apparent age (years) of the Labrador Sea Water component of upper NADW outflow in the model ocean. Because the CFC-11/CFC-12 ratio has remained approximately constant (near 0.57) since 1975 (Figure 3), we give only an upper bound for the age of water exposed to the atmosphere since that time. In addition, significant atmospheric traces of CFC-11 do not appear until the 1950s, so we can, at best, trace water parcels that are around 35 years old.

An assumption that the ocean surface is instantaneously in saturated CFC equilibrium with the atmosphere is seen to grossly overestimate the flux of CFC-11 and CFC-12 into the ocean. Deep and bottom water CFC-11 concentrations in the central Arctic and Southern Oceans can be as much as 10 times too large when the model ocean is assumed to maintain saturated CFC equilibrium at all times. The use of a classical air-sea gas exchange formula (even one with a simplified gas transfer velocity that is independent of wind speed) is seen to greatly improve the CFC simulations at depth. In addition, the model reproduces many of the observed trends in surface CFC concentrations, namely, undersaturation in regions of deep convective overturn and near-surface upwelling and supersaturation in the summer mixed layer. The convected layer undersaturations can be as much as 50% during a deep wintertime overturning event, though more typical undersaturation levels are in the range 10–35%. This degree of undersaturation agrees well with a range of observational studies in the winter mixed layer. A consideration of sea ice coverage further improves the CFC-11 simulations in the polar deepwater formation regions. The presence of sea ice acts to limit the area of seawater exposed to atmospheric forcing in the winter hemisphere. Percentage of saturated equilibrium can be as weak as 25% in regions persistently covered with sea ice, which is in approximate agreement with observed CFC concentrations in polar surface waters. A consideration of surface wind speeds in the calculation of the air-sea gas piston velocity is seen to increase the surface CFC fluxes over the subpolar oceans. Equilibration timescales as fast as 10–15 days are calculated over high wind speed regions of the North Atlantic and Southern Oceans

during winter, as much as halving the equilibration timescale assumed in the CF2 experiment. In polar and tropical regions the wind speed dependent piston velocity is slower than the constant rate assumed in experiment CF2 ($k_2 = 10.6$ cm/h), yielding higher undersaturation levels in regions of upwelling and vertical convection.

Deep and bottom water outflows from convectively active regions are found to be characterized by significant levels of CFC-11 and CFC-12 concentration. In particular, bottom water formed adjacent to Antarctica in the Weddell Sea is seen to spread northward into the deep South Atlantic and eastward into the Indian Ocean. The ventilation of the South Atlantic Ocean by CFC-enriched bottom water is far too strong when surface CFC concentrations are forced to maintain saturated equilibrium levels. With more realistic air-sea gas forcing the concentration of CFC-11 in the northward flowing WSBW remains marginally too strong, with a western boundary signature of 0.03 pmol/kg reaching 25°S in late 1983. This is around 4 years earlier than the SAVE measurement of CFC-enriched WSBW (0.034 pmol/kg) at 25°S during March 1988 [Weiss *et al.*, 1993]. In the deep Pacific Ocean, CFC-tagged bottom water formed in the Ross Sea flows into the Southwest and Southeast Pacific Basins, with the subsequent northward spreading somewhat weaker than the corresponding South Atlantic flows. Like the bottom water generated in the Weddell Sea, concentrations in the RSBW outflow are very sensitive to the parameterization of air-sea gas exchange. From a comparison between the simulated and observed CFC-11 concentrations at the Greenwich meridian it seems that too much convective overturn persists in the Southern Ocean at 55°S–70°S, with unrealistically deep penetration of young CFC-enriched waters. This is because not enough older (CFC deprived) water recirculates and upwells into the Southern Ocean. More upwelled circumpolar deep water in the region would weaken the CFC-11 concentrations significantly, not only because the older water would contribute to a lower CFC mixture, but also because the convective activity in the region would be suppressed due to the stabilization of the water column.

A reasonable representation of oceanic CFC is achieved in the convected water column in the North Atlantic Ocean. In contrast, deep waters that have left the convective area with the model ocean currents are found to be deficient in CFC-11. This is because of the relatively long advective timescale for the modeled NADW to flow to the equator (30–35 years) compared with observed ocean estimates (23 years). The slow advective timescale for NADW outflow does not seem to be due to underestimated mean flows in the deep model levels. Rather, it is because the NADW outflow from the Labrador and Greenland Seas includes a loop eastward into the Northeastern Atlantic Basin. This eastward excursion of some of the NADW increases the required equatorial journey by around 4000 km. Consequently, the water eventually arriving in the deep tropical Atlantic is somewhat older than it would have been had it taken a shortcut southward from the Labrador Sea. On the basis of the CFC-11/CFC-12 ratio of water arriving at the South American continent during 1988 (at 10°N) an age estimate of 32 years is given for that portion of the water that was originally exposed to atmospheric conditions in the Labrador Sea. This age estimate can be used to extrapolate the degree of dilution of the upper NADW arriving at 10°N

assuming that the dilution is principally from water that is CFC free. On the basis of the atmospheric history of CFC-11 and a knowledge of surface saturation levels in the regions of NADW formation, we found the water at 10°N to be diluted about 3.5 times by CFC-free waters (that is, the mixture arriving in the tropical Atlantic is around 30 parts NADW and 70 parts older, recirculated CFC-free water). The dilution in the model could come from vertical diffusion since the vertical resolution is coarse in the deeper model levels, so that an outflowing CFC signature at a particular level is likely to be eroded by the relatively deficient CFC waters above and below it.

The potential for CFCs to be used as constraints in ocean circulation models has been demonstrated by our study. The conventional hydrographic tracers (temperature and salinity) can only provide so much information in the context of model validation and circulation diagnosis. The uptake of two extra tracers over a 60-year period is computationally inexpensive compared with the long millennia timescales required to properly equilibrate ocean GCMs. In the context of the global carbon cycle, circulation models are typically validated using to reproduce anthropogenic ^{14}C invasion before being used to study oceanic CO_2 uptake [e.g., Maier-Reimer and Hasselmann, 1987; Sarmiento *et al.*, 1992]. Using CFC-11 and CFC-12 as validation tracers would allow a separation of deep ventilation effects from biological processes. Even though the CFC ventilation of the ocean is relatively recent and present-day CFC data are only useful in the context of ocean circulation over the decadal to inter-decadal timescale, in the future, more and more structure will evolve in the deep ocean measurements. This should mean a wealth of validation data for the ocean circulation modeler.

Acknowledgments. This research was partially supported by EPOCH CEE grant EVSV CT92/0124. The model computations were carried out on the CNES (Centre National d'Etudes Spatiales) Cray-2 machine and the CSIRO Cray-YMP 4E/369. This study contributes to the CSIRO Climate Change Research Program and was partly funded through Australia's National Greenhouse Research Program. The authors gratefully acknowledge the GFDL for providing a copy of the Modular Ocean Model and the climatological forcing data sets. The CFC atmospheric histories were kindly provided by Mark Warner and John Bullister. M.H.E. acknowledges discussions and correspondence with John Bullister, Keith Dixon, Peter Liss, Stefan Rahmstorf, Robbie Toggweiler, Mark Warner, and Ray Weiss.

References

- Broecker, W. S., and T. H. Peng, *Tracers in the Sea*, 690 pp., Lamont-Doherty Geological Observatory, Palisades, N. Y., 1982.
- Bryan, K., A numerical method for the study of the circulation of the World Ocean, *J. Comput. Phys.*, **3**, 347–376, 1969.
- Bryan, K., and L. J. Lewis, A water mass model of the World Ocean, *J. Geophys. Res.*, **84**, 2503–2517, 1979.
- Bullister, J. L., Chlorofluorocarbons as time-dependent tracers in the ocean, *Oceanography*, 12–17, November 1989.
- Bullister, J. L., and R. F. Weiss, Anthropogenic chlorofluorocarbons in the Greenland and Norwegian Seas, *Science*, **221**, 265–268, 1983.
- Comiso, J. C., C. R. McClain, C. W. Sullivan, J. P. Ryan, and C. L. Leonard, Coastal zone color scanner pigment concentrations in the southern ocean and relationships to geophysical surface features, *J. Geophys. Res.*, **98**, 2419–2451, 1993.
- Cox, M. D., A primitive equation, three-dimensional model of the ocean, *Tech. Rep. 1*, 143 pp., Ocean Group, Geophys. Fluid Dyn. Lab., Princeton, N. J., 1984.

- Cunnold, D. M., R. G. Prinn, R. A. Rasmussen, P. G. Simmonds, F. N. Alyea, C. A. Cardelino, A. J. Crawford, P. J. Fraser, and R. D. Rosen, The atmospheric lifetime experiment, 3, Lifetime methodology and application to three years of CFCl_3 data, *J. Geophys. Res.*, **88**, 8379–8400, 1983a.
- Cunnold, D. M., R. G. Prinn, R. A. Rasmussen, P. G. Simmonds, F. N. Alyea, C. A. Cardelino, A. J. Crawford, P. J. Fraser, and R. D. Rosen, The atmospheric lifetime experiment, 4, Results for CF_2Cl_2 based on three years data, *J. Geophys. Res.*, **88**, 8401–8414, 1983b.
- Doney, S. C., and J. L. Bullister, A chlorofluorocarbon section in the eastern North Atlantic, *Deep Sea Res.*, **39**, 1857–1883, 1992.
- England, M. H., On the formation of Antarctic Intermediate and Bottom Water in ocean general circulation models, *J. Phys. Oceanogr.*, **22**, 918–926, 1992.
- England, M. H., Representing the global-scale water masses in ocean general circulation models, *J. Phys. Oceanogr.*, **23**, 1523–1552, 1993.
- England, M. H., J. S. Godfrey, A. C. Hirst, and M. Tomczak, The mechanism for Antarctic Intermediate Water renewal in a World Ocean model, *J. Phys. Oceanogr.*, 1553–1560, 1993.
- Esbenson, S. K., and Y. Kushnir, The heat budget of the global ocean: An atlas based on estimates from surface marine observations, *Rep. 29*, Climate Res. Inst., Oregon State Univ., Corvallis, 1981.
- Fine, R. A., Circulation of Antarctic Intermediate Water in the south Indian Ocean, *Deep Sea Res.*, **40**, 2021–2042, 1993.
- Gordon, A. L., R. F. Weiss, W. M. Smethie, and M. J. Warner, Thermocline and intermediate water communication between the South Atlantic and Indian Oceans, *J. Geophys. Res.*, **97**, 7223–7240, 1992.
- Haney, R. L., Surface thermal boundary condition for ocean circulation models, *J. Phys. Oceanogr.*, **1**, 241–248, 1971.
- Hellerman, S., and M. Rosenstein, Normal monthly wind stress over the World Ocean with error estimates, *J. Phys. Oceanogr.*, **13**, 1093–1104, 1983.
- Hirst, A. C., and J. S. Godfrey, The role of the Indonesian throughflow in a global ocean GCM, *J. Phys. Oceanogr.*, **23**, 1057–1086, 1993.
- Krissell, M., and D. W. R. Wallace, Arctic Ocean ventilation studied with a suite of anthropogenic halocarbon tracers, *Science*, **242**, 746–749, 1988.
- Levitus, S., Climatological atlas of the World Ocean, *Prof. Pap. 13*, 173 pp., Natl. Oceanic and Atmos. Admin., U.S. Dep. of Comm., Washington D. C., 1982.
- Levitus, S., Annual cycle of temperature and heat storage in the World Ocean, *J. Phys. Oceanogr.*, **14**, 727–746, 1984.
- Levitus, S., Annual cycle of salinity and salt storage in the World Ocean, *J. Phys. Oceanogr.*, **16**, 322–343, 1986.
- Liss, P. S., and L. Merlivat, Air-sea exchange rates: Introduction and synthesis, in *The Role of Air-Sea Exchange in Geochemical Cycling*, edited by P. Buat-Menard, pp. 113–127, D. Reidel, Norwell, Mass., 1986.
- Maier-Reimer, E., and K. Hasselmann, Transport and storage of CO_2 in the ocean—An inorganic ocean circulation carbon cycle model, *Clim. Dyn.*, **2**, 63–90, 1987.
- Manabe, S., R. J. Stouffer, M. J. Spelman, and K. Bryan, Transient responses of a coupled ocean-atmosphere model to gradual changes of atmospheric carbon dioxide, Part I, Annual mean response, *J. Climate*, **4**, 785–818, 1991.
- Manabe, S., M. J. Spelman, and R. J. Stouffer, Transient responses of a coupled ocean-atmosphere model to gradual changes of atmospheric carbon dioxide, Part II, Seasonal response, *J. Climate*, **5**, 105–126, 1992.
- Marti, O., Etude de l'océan mondial: Modélisation de la circulation et du transport des traceurs anthropiques, 201 pp., thèse de Doct., l'Univ. Paris VI, Paris, France, 1992.
- Pacanowski, R. C., K. W. Dixon, and A. Rosati, The GFDL Modular Ocean Model Users Guide version 1.0, *Tech. Rep. 2*, 46 pp., Ocean Group, Geophys. Fluid Dyn. Lab., Princeton, N. J., 1991.
- Parkinson, C. L., J. C. Comiso, H. J. Zwally, D. J. Cavalieri, P. Gloersen, and W. J. Campbell, Arctic sea ice, 1973–1976: Satellite passive-microwave observations, *NASA Spec. Publ.*, **SP-489**, 296 pp., 1987.
- Pickart, R. S., N. G. Hogg, and W. M. Smethie, Determining the strength of the Deep Western Boundary Current using the chlorofluoromethane ratio, *J. Phys. Oceanogr.*, **19**, 940–951, 1989.
- Rahmstorf, S., and J. Willebrand, The role of temperature feedback in stabilising the thermohaline circulation, *J. Phys. Oceanogr.*, in press, 1994.
- Sarmiento, J. L., A simulation of bomb tritium entry into the Atlantic Ocean, *J. Phys. Oceanogr.*, **13**, 1924–1939, 1983.
- Sarmiento, J. L., J. C. Orr, and U. Siegenthaler, A perturbation simulation of CO_2 uptake in an ocean general circulation model, *J. Geophys. Res.*, **97**, 3621–3645, 1992.
- Schlosser, P., J. L. Bullister, and R. Bayer, Studies of deep water formation and circulation in the Weddell Sea using natural and anthropogenic tracers, *Mar. Chem.*, **35**, 97–122, 1991.
- Smethie, W. M., Tracing the thermohaline circulation in the western North Atlantic using chlorofluorocarbons, *Prog. Oceanogr.*, **31**, 51–99, 1993.
- Stouffer, R. J., S. Manabe, and K. Bryan, Interhemispheric asymmetry in climate response to a gradual increase of atmospheric CO_2 , *Nature*, **342**, 660–662, 1989.
- Toggweiler, J. R., K. Dixon, and K. Bryan, Simulations of radiocarbon in a coarse-resolution world ocean model, 1, Steady state prebomb distributions, *J. Geophys. Res.*, **94**, 8217–8242, 1989a.
- Toggweiler, J. R., K. Dixon, and K. Bryan, Simulations of radiocarbon in a coarse-resolution world ocean model, 2, Distributions of bomb-produced carbon 14, *J. Geophys. Res.*, **94**, 8243–8264, 1989b.
- Wallace, D. W. R., and J. R. N. Lazier, Anthropogenic chlorofluoromethanes in newly formed Labrador Sea Water, *Nature*, **332**, 61–63, 1988.
- Wallace, D. W. R., and R. M. Moore, Vertical profiles of CCl_3F (F-11) and CCl_2F_2 (F-12) in the Central Arctic Ocean Basin, *J. Geophys. Res.*, **90**, 1155–1166, 1985.
- Wanninkhof, R., Relationship between wind speed and gas exchange over the ocean, *J. Geophys. Res.*, **97**, 7373–7382, 1992.
- Warner, M. J., and R. F. Weiss, Solubilities of chlorofluorocarbons 11 and 12 in water and seawater, *Deep Sea Res.*, **32**, 1485–1497, 1985.
- Warner, M. J., and R. F. Weiss, Chlorofluoromethanes in South Atlantic Antarctic Intermediate Water, *Deep Sea Res.*, **39**, 2053–2075, 1992.
- Weiss, R. F., J. L. Bullister, R. H. Gammon, and M. J. Warner, Atmospheric chlorofluoromethanes in the deep equatorial Atlantic, *Nature*, **314**, 608–610, 1985.
- Weiss, R. F., M. J. Warner, P. K. Salameh, F. A. Van Woy, and K. G. Harrison, *South Atlantic Ventilation Experiment: SIO Chlorofluorocarbon Measurements*, *Ref. 93-49*, 466 pp., Scripps Inst. of Oceanogr., La Jolla, Calif., 1993.
- Welander, P., Thermohaline effects in the ocean circulation and related simple models, in *Large-Scale Transport Processes in the Oceans and Atmosphere*, edited by J. Willebrand and D. L. T. Anderson, pp. 163–200, D. Reidel, Norwell, Mass., 1986.

M. H. England, CSIRO Division of Atmospheric Research, PMB1, Mordialloc, 3195, Victoria, Australia. (e-mail: mhe@dar.csiro.au)

V. Garçon and J.-F. Minster, Groupe de Recherche de Géodésie Spatiale, CNRS, 18 av. E. Belin, 31055 Toulouse, France. (e-mail: garcon@pontos.cnes.fr; minster@pontos.cnes.fr)

(Received December 20, 1993; revised July 6, 1994; accepted August 23, 1994.)